NASA TECHNICAL NOTE

NASA TN D-5378

AERODYNAMIC CHARACTERISTICS IN PITCH OF A 1/7-SCALE MODEL OF A TWO- AND THREE-STAGE ROCKET CONFIGURATION AT MACH NUMBERS OF 0.4 TO 4.63

*by William F. Hinson, Richard A. Langhans,
and Roger H. Fournier*

*Langley Research Center
Langley Station, Hampton, Va.*

NATIONAL AERONAUTICS AND SPACE ADMINISTRATION • WASHINGTON, D. C. • AUGUST 1969

1. Report No. NASA TN D-5378	2. Government Accession No.	3. Recipient's Catalog No.
4. Title and Subtitle AERODYNAMIC CHARACTERISTICS IN PITCH OF A 1/7-SCALE MODEL OF A TWO- AND THREE-STAGE ROCKET CONFIGURATION AT MACH NUMBERS OF 0.4 TO 4.63		5. Report Date August 1969
		6. Performing Organization Code
7. Author(s) William F. Hinson, Richard A. Langhans, and Roger H. Fournier		8. Performing Organization Report No. L-6614
9. Performing Organization Name and Address NASA Langley Research Center Hampton, Va. 23365		10. Work Unit No. 709-09-00-01-23
		11. Contract or Grant No.
12. Sponsoring Agency Name and Address National Aeronautics and Space Administration Washington, D.C. 20546		13. Type of Report and Period Covered Technical Note
		14. Sponsoring Agency Code

15. Supplementary Notes

16. Abstract

    An investigation has been conducted to determine the longitudinal stability characteristics of the upper two- and three-stage combinations of a four-stage solid-propellant unguided rocket research vehicle. The stages tested were stabilized by trapezoidal cruciform fins. Test Mach number range for the three-stage configuration was 0.4 to 1.0; for the two-stage configuration, 0.4 to 4.63. Angle-of-attack range was approximately -4° to 14°. Reynolds number ranged from 1.5×10^6 to 3.4×10^6 per foot $(4.92 \times 10^6$ to 11.14×10^6 per meter). The general aerodynamic characteristics of normal-force, pitching-moment, and drag coefficients as a function of angle of attack and Mach number are presented.

17. Key Words Suggested by Author(s) Four-stage solid-propellant research vehicles Aerodynamic coefficients Stability criteria	18. Distribution Statement Unclassified – Unlimited		
19. Security Classif. (of this report) Unlassified	20. Security Classif. (of this page) Unclassified	21. No. of Pages 40	22. Price* $3.00

AERODYNAMIC CHARACTERISTICS IN PITCH OF A 1/7-SCALE MODEL

OF A TWO- AND THREE-STAGE ROCKET CONFIGURATION

AT MACH NUMBERS OF 0.4 TO 4.63

By William F. Hinson, Richard A. Langhans,
and Roger H. Fournier
Langley Research Center

SUMMARY

An investigation has been conducted to determine the longitudinal stability characteristics of the upper two- and three-stage combinations of a four-stage solid-propellant unguided rocket research vehicle. The stages tested were stabilized by trapezoidal cruciform fins. Test Mach number range for the three-stage configuration was 0.4 to 1.0; for the two-stage configuration, 0.4 to 4.63. Angle-of-attack range was approximately -4° to 14°. Reynolds number ranged from 1.5×10^6 to 3.4×10^6 per foot $\left(4.92 \times 10^6 \text{ to } 11.14 \times 10^6 \text{ per meter}\right)$. The general aerodynamic characteristics of normal-force, pitching-moment, and drag coefficients as a function of angle of attack and Mach number are presented.

INTRODUCTION

In the past decade several flight experiments have been conducted with an unguided solid-propellant rocket research vehicle which consisted of an Honest John, Nike, and TX-77 rocket motors as stages 1, 2, and 3, respectively. Vehicle geometry and number of stages above stage 3 have varied depending upon the particular flight experiment. At present a four-stage version of the vehicle is being utilized in the Pacemaker flight project to study spacecraft heat-shield materials. The fourth stage consists of a Recruit solid-propellant rocket motor and spacecraft.

Several flights have been conducted in the project; two of the experiments are reported in references 1 and 2. During these and other flights of this vehicle, some trajectory deviations were noted during the flight of the upper three stages. These deviations were not critical to the experiment but did cause some changes from the desired-test-phase environmental conditions. Therefore, to exercise more control of the conditions during the test phase for follow-on flights, it was found necessary to ignite the third stage by ground command. Ground command procedures had to be generated by preflight computer trajectory analysis which required the use of aerodynamic coefficients over the

particular flight regime. Experimental aerodynamic coefficients for the present vehicle geometry in this flight regime were not available for the computer study. Since some of the aforementioned trajectory deviations could be attributable to aerodynamic anomalies, it was required that experimental aerodynamic coefficients be obtained for the upper three- and two-stage configurations through the speed ranges which these stages would experience in flight. References 3 and 4 present experimental supersonic aerodynamic coefficients for similar configurations; however, the fourth-stage geometry differs markedly from that reported herein.

A 1/7-scale model of the present upper two stages was tested over a Mach number range of 0.4 to 4.63, the upper three stages being tested over a Mach number range of 0.4 to 1.0. Angles of attack were approximately -4° to 14°. Reynolds number, depending upon Mach number, varied between 1.5×10^6 and 3.4×10^6 per foot $\left(4.92 \times 10^6 \text{ and } 11.14 \times 10^6 \text{ per meter}\right)$.

SYMBOLS

The aerodynamic force and moment data are referred to the body-axis system with the moment reference center located at body station 36 for model 1 and station 57 for model 2. (See fig. 1.)

A cross-sectional area of model maximum cylinder diameter

C_A axial-force coefficient $\left(\text{does not include } C_{A,b}\right)$, $\dfrac{\text{Axial force}}{q_\infty A}$

$C_{A,b}$ base axial-force coefficient, $\dfrac{\text{Base axial force}}{q_\infty A}$

$C_{A,o}$ axial-force coefficient at $\alpha = 0^{\circ}$

C_m pitching-moment coefficient, $\dfrac{\text{Pitching moment}}{q_\infty Ad}$

C_{m_α} slope of pitching-moment curve through $\alpha = 0^{\circ}$

C_N normal-force coefficient, $\dfrac{\text{Normal force}}{q_\infty A}$

C_{N_α} slope of normal-force curve through $\alpha = 0^{\circ}$

d maximum cylinder diameter of particular model

M_∞ free-stream Mach number

q_∞ free-stream dynamic pressure

α angle of attack of model center line

x_{cp} center of pressure measured from model base,

$$\frac{x_{cp} - x_{moment\ reference}}{d} = -\frac{C_{m\alpha}}{C_{N\alpha}}\bigg|_{\alpha=0^0}$$

Fin designations:

F_1 fins for rear stage of model 2, represents a full-scale area of 2.75 ft^2
           (0.255 m^2) exposed area per panel

F_2 fins for rear stage of model 2, represents a full-scale area of 3.25 ft^2
           (0.302 m^2) exposed area per panel

F_3 fins for rear stage of model 1, represents a full-scale area of 2.0 ft^2
           (0.186 m^2) exposed area per panel

F_4 fins for rear stage of model 1, represents a full-scale area of 2.5 ft^2
           (0.232 m^2) exposed area per panel

APPARATUS AND METHODS

Models

A sketch of the models tested, the model designations, and detailed dimensions are shown in figures 1 and 2. Model photographs are presented in figure 3. The model body was constructed from aluminum; the fins were constructed from stainless steel. Model 1 represents the upper two stages and spacecraft of the operational four-stage solid propellant Pacemaker unguided rocket vehicle. Model 2 represents the upper three stages and spacecraft of the same vehicle. For purposes of clarity, the model stages are labeled 1, 2, and 3, stage 3 being the uppermost stage with the scaled spacecraft attached. (See fig. 1.) The spacecraft nose is a hemisphere segment tangent to a 6^0 half-angle cone frustum which is followed by a short cylinder. The cylinder diameter is larger than the stage 3 diameter; therefore, an inverse cone frustum with half-angle of about 3^0 is used

to connect the spacecraft to stage 3. Stage 3 is stabilized by a 10° half-angle flare and is attached to stage 2 by an inverse cone frustum of approximately 5° half-angle.

Fin dimensions and designations are presented in figure 2. For stage 1 fins F_1 and F_2 were sized to represent a full-scale area of 2.75 ft^2 (0.255 m^2) and 3.25 ft^2 (0.302 m^2) exposed area per panel. For stage 2, fins F_3 and F_4 were sized to represent a full-scale area of 2 ft^2 (0.186 m^2) and 2.5 ft^2 (0.232 m^2) of exposed area per panel. For model 2 the fins were interdigitated. Fins F_1 and F_3 were scaled from standard flight fins used with the Nike and TX-77 rocket motor, respectively. The larger fins F_2 and F_4 were scaled from proposed full-scale fins which represents an area increase of 1/2 square foot per panel over the standard fins.

Tunnels

The investigation was conducted in the Langley Unitary Plan wind tunnel and also in the Langley 8-foot transonic pressure tunnel. Because of model length, model 2 was tested only in the Langley 8-foot transonic pressure tunnel. Both tunnels are variable-pressure continuous-flow tunnels. A more detailed description of the facilities is presented in reference 5.

Test Conditions

Model 1 was tested over a Mach number range from 0.4 to 4.63. No data were obtained between Mach 1 and 2 because the bow shock was reflecting off the tunnel wall back to the model body in front of the stabilizing fins. Model 2 was tested over a Mach number range of 0.4 to 1.0. Both models with various fin configurations and with no fins were tested through an angle-of-attack range of about -4° to 14°. In all tests the models had a fixed transition strip attached approximately 1 inch back from the nose and 1/4 inch back from the leading edge of each fin panel. The strip was approximately 0.1 inch wide and was composed of No. 60 carborundum grains set in an adhesive. Free-stream Reynolds number per foot for the test range was from 1.5×10^6 to 3.4×10^6 per foot $\left(4.92 \times 10^6 \text{ to } 11.14 \times 10^6 \text{ per meter}\right)$. Figure 4 shows the Reynolds number range as a function of Mach number.

Measurements

Aerodynamic forces and moments were measured by means of a six-component electrical strain-gage balance mounted within the model shell. The balance was rigidly fastened to a sting support which was in turn fastened to the tunnel support system. Two base-pressure measurements were made, one approximately one-half the distance between the sting surface and the outside of the model shell, and one close to the outside surface of the model shell. These two measurements were averaged to obtain the base pressure.

4

RESULTS AND DISCUSSION

The basic aerodynamic characteristics for the configurations tested are presented in figures 5 and 6. Summarization of the basic data is presented in faired curve form in figure 7. The pitching-moment data are presented about the balance pitch center for each configuration which is 66.6 and 76.6 percent of body length measured from the model nose for models 1 and 2, respectively. These pitch centers were selected to facilitate model design and do not indicate a realistic flight moment reference; this reference would be the flight-vehicle center of gravity which is approximately 60 percent of body length measured from the nose.

Variations to model configurations were restricted to changes in fin size. The results presented in figures 5 and 6 show that the addition of fins to the model body and/or increasing fin areas resulted in appreciable increments of normal force and pitching moment. In general, the normal-force data are linear up to about 2° for both models at all Mach numbers. Above 2° in most cases, small increases occur in the slope of the C_N curve. This trend is characteristic of long slender bodies and is associated with viscous body lift as presented in reference 6. The pitching-moment-coefficient curves are also linear to about 2°. With model 1 in figures 5(b), 5(c), and 5(g) to 5(k) at Mach numbers of 0.6, 0.8, and 2.0 to 4.63, the pitching-moment slope changes from negative to positive at about $\alpha = 8^\circ$. This slope change is partly due to the placement of the pitch-moment center too far rearward and at supersonic speeds partly due to loss of fin effectiveness with Mach number increase. With model 2, figure 6 at $M_\infty = 0.4$ to 1.0, the slope change of C_m is due to the fins not being adequate to provide a stabilizing moment about the balance moment center.

The slopes of C_m and C_N through $\alpha = 0^\circ$ were used to compute the center of pressure x_{cp} values which are presented in figures 7(b) and 7(d). For model 1 with the fins on, the x_{cp} movement toward the model base was greatest at subsonic speeds. As usual, an increase in Mach number above 1 results in a forward movement in x_{cp}. With the standard fin F_3 for model 1, the forward movement of x_{cp} from 0.4 to 4.63 was about 30 percent of the body length. (See fig. 7(b).)

The base drag coefficient $C_{A,b}$ (in this case the axial force) has been subtracted from the total-drag measurements, that is, C_A. As would be expected, the addition of fins and/or increased fin area results in appreciable increases in C_A. In general, the C_A values show a small increase with increasing angle of attack. As usual, the $C_{A,o}$ values indicate a sharp rise in the transonic region with a gradual decrease with increasing Mach number as shown in figure 7(a) with model 1.

Base drag coefficients are presented in figure 8. The subsonic data suggest that the fins cause boundary-layer and/or wake conditions which result in a reduction of base drag. At supersonic Mach numbers the fins cause flow conditions which result in an increase in base drag. In figure 8(a) with model 1, it is shown that the fin effect on base drag diminishes with increasing Mach number.

CONCLUDING REMARKS

An investigation has been conducted to determine the longitudinal stability characteristics of the upper two- and three-stage combinations of a four-stage solid-propellant unguided rocket research vehicle. The stages tested were stabilized by trapezoidal cruciform fins. Test Mach number range for the three-stage configuration was 0.4 to 1.0; for the two-stage configuration, 0.4 to 4.63. The angle-of-attack range was approximately -4° to 14°. Reynolds number ranged from 1.5×10^6 to 3.4×10^6 per foot $\left(4.92 \times 10^6 \text{ to } 11.14 \times 10^6 \text{ per meter}\right)$.

The addition of fins to the body and/or increasing fin areas resulted in appreciable increments of normal force and pitching moment. This condition also results in appreciable increases in the axial-force coefficients. In general, the axial-force coefficients show a small increase with increasing angle of attack. The subsonic data suggest that the fins cause boundary-layer and/or wake conditions which result in a reduction of base drag. At supersonic Mach numbers the fins cause flow conditions which result in an increase in base drag. The fin effect on base drag diminishes with increasing Mach number.

Langley Research Center,
National Aeronautics and Space Administration,
Langley Station, Hampton, Va., June 5, 1969,
709-09-00-01-23.

REFERENCES

1. Graves, Randolph A., Jr.; and Witte, William G.: Flight-Test Analysis of Apollo Heat-Shield Material Using the Pacemaker Vehicle System. NASA TN D-4713, 1968.

2. Walton, Thomas E., Jr.; Witte, William G.; and O'Hare, Brian J.: Flight Investigation of the Effects of Apollo Heat-Shield Singularities on Ablator Performance. NASA TN D-4791, 1968.

3. Robinson, Ross B.: Effects of Body and Fin Deflections on the Aerodynamic Characteristics in Pitch of a 0.065-Scale Model of a Four-Stage Rocket Configuration at Mach Numbers of 1.41 and 1.82. NASA TN D-37, 1959.

4. Gregory, Donald T.; and Carraway, Ausley B.: Investigation of the Static Longitudinal Stability and Roll Characteristics of a Three-Stage Missile Configuration at Mach Numbers From 1.77 to 2.87. NASA TM X-124, 1959.

5. Schaefer, William T., Jr.: Characteristics of Major Active Wind Tunnels at the Langley Research Center. NASA TM X-1130, 1965.

6. Polhamus, Edward C.: Effect of Nose Shape on Subsonic Aerodynamic Characteristics of a Body of Revolution Having a Fineness Ratio of 10.94. NACA RM L57F25, 1957.
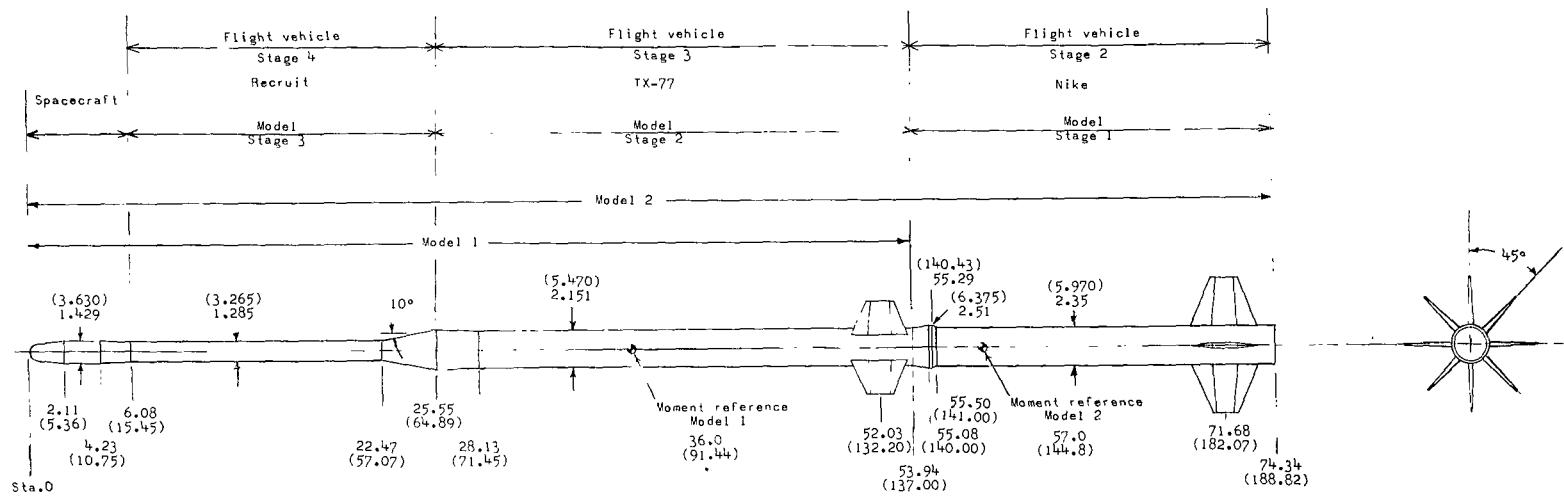
Figure 1.- Sketch of test models. Linear dimensions are given in inches and parenthetically in centimeters.
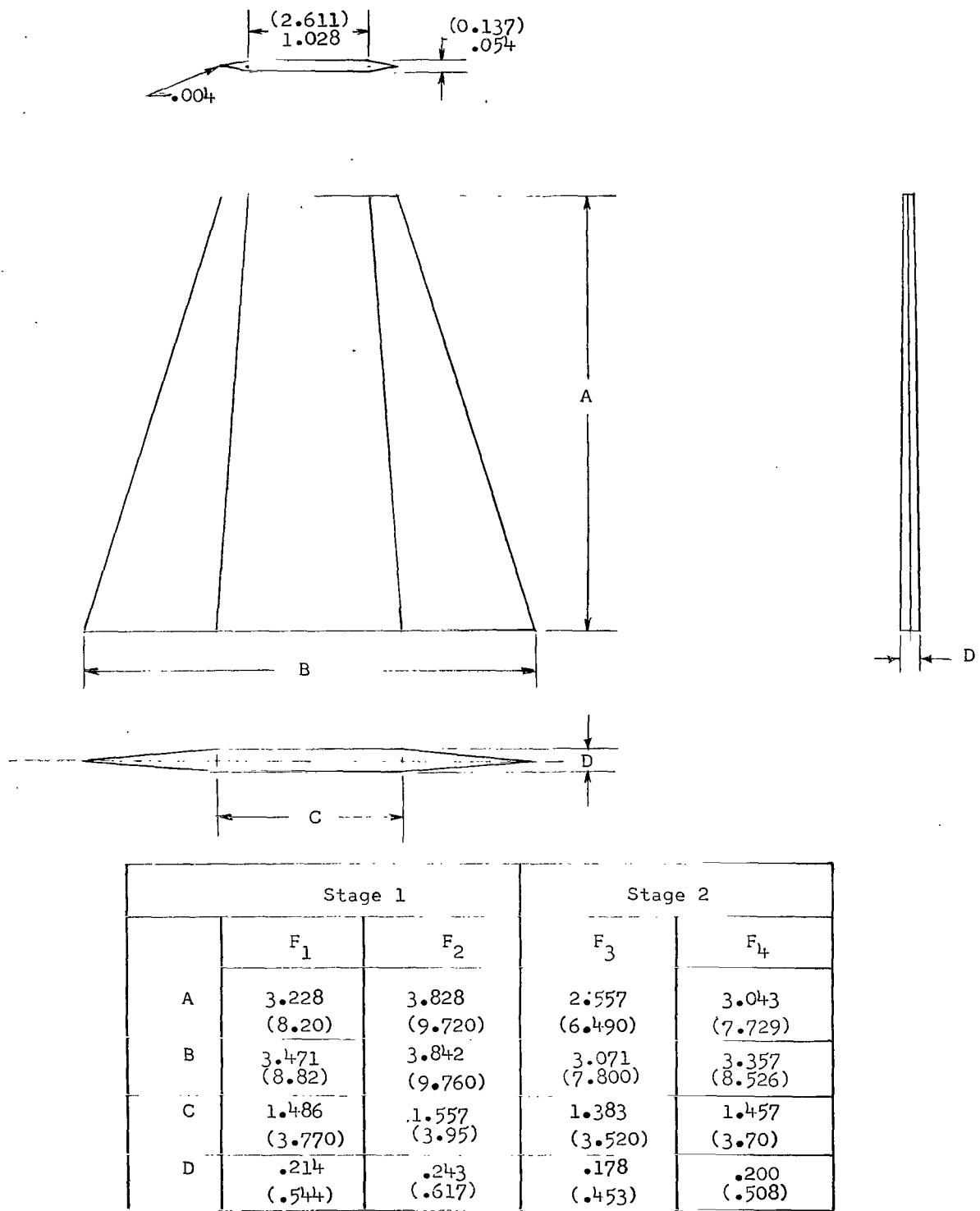
Figure 2.- Model fin dimensions and designations. Dimensions are given in inches and parenthetically in centimeters.

	Stage 1		Stage 2	
	F_1	F_2	F_3	F_4
A	3.228 (8.20)	3.828 (9.720)	2.557 (6.490)	3.043 (7.729)
B	3.471 (8.82)	3.842 (9.760)	3.071 (7.800)	3.357 (8.526)
C	1.486 (3.770)	1.557 (3.95)	1.383 (3.520)	1.457 (3.70)
D	.214 (.544)	.243 (.617)	.178 (.453)	.200 (.508)
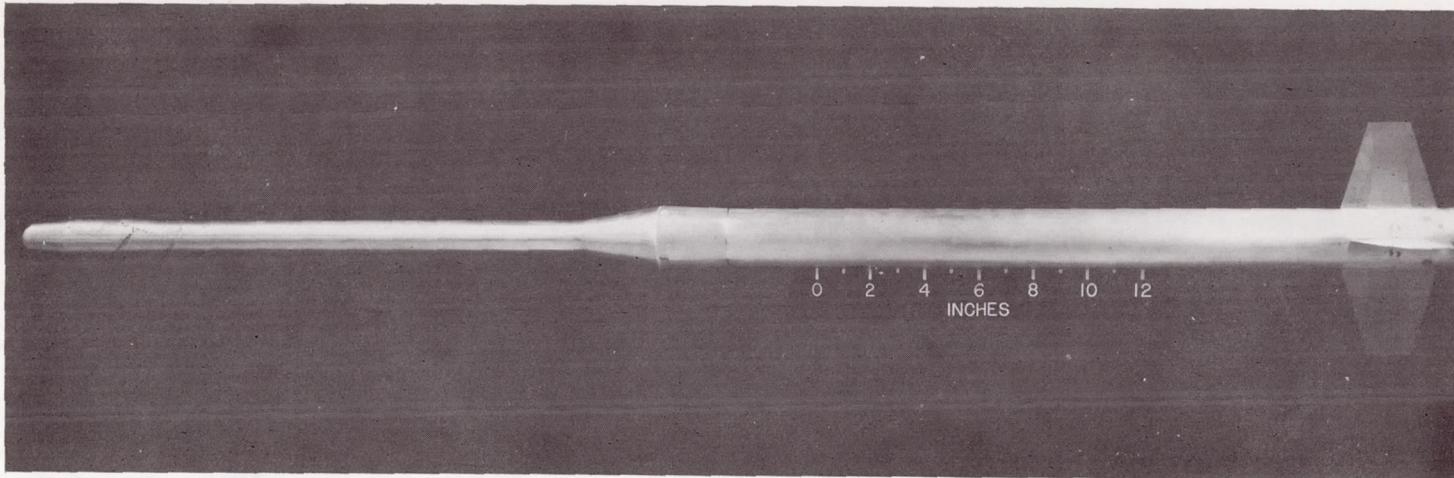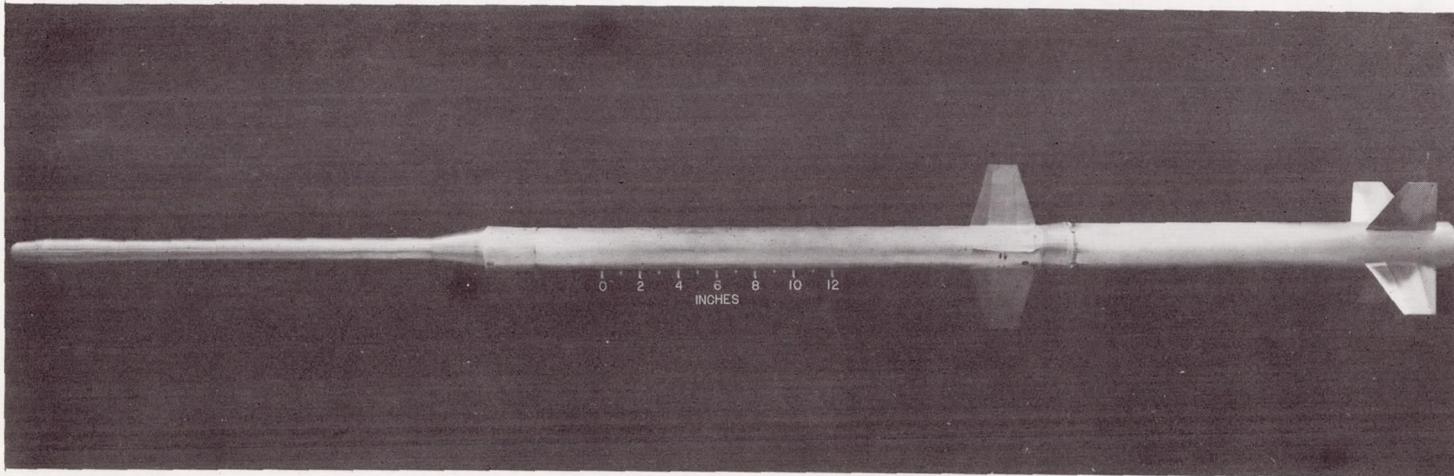
(a) Model 1.

(b) Model 2.

Figure 3.- Photographs of test models.

L-69-5228
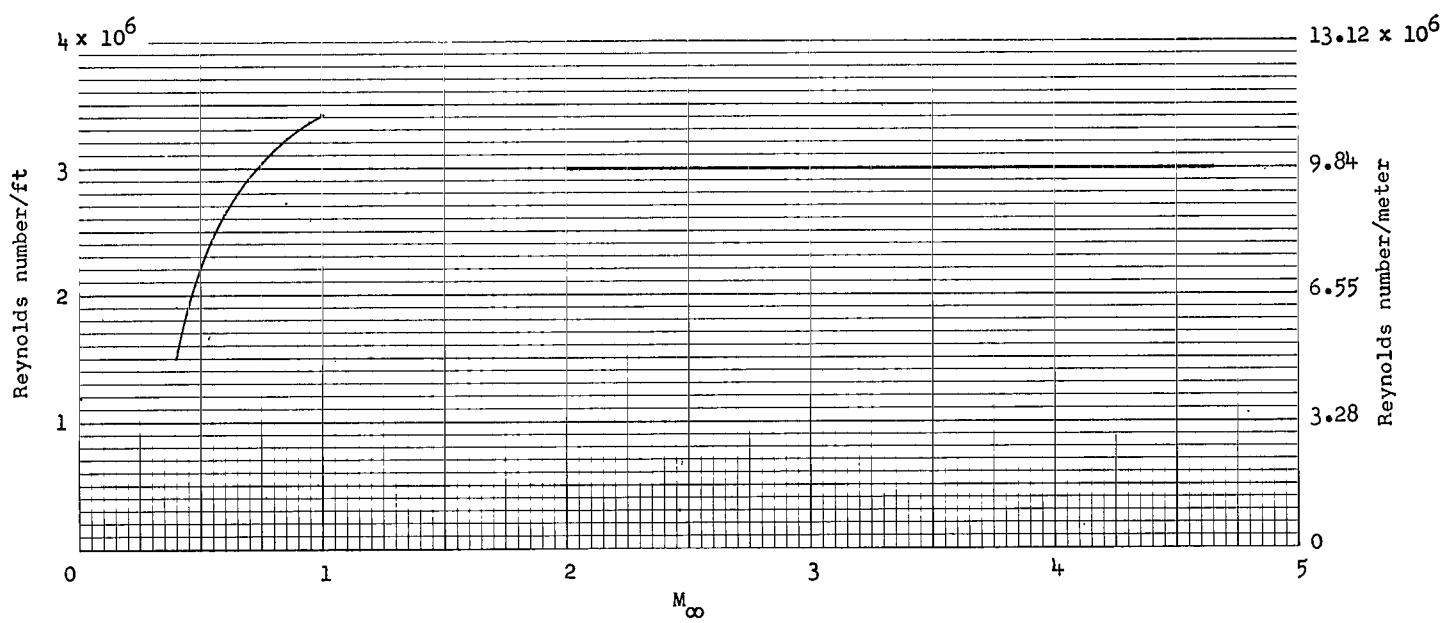
Figure 4.- Variation of test Reynolds number per foot with Mach number.
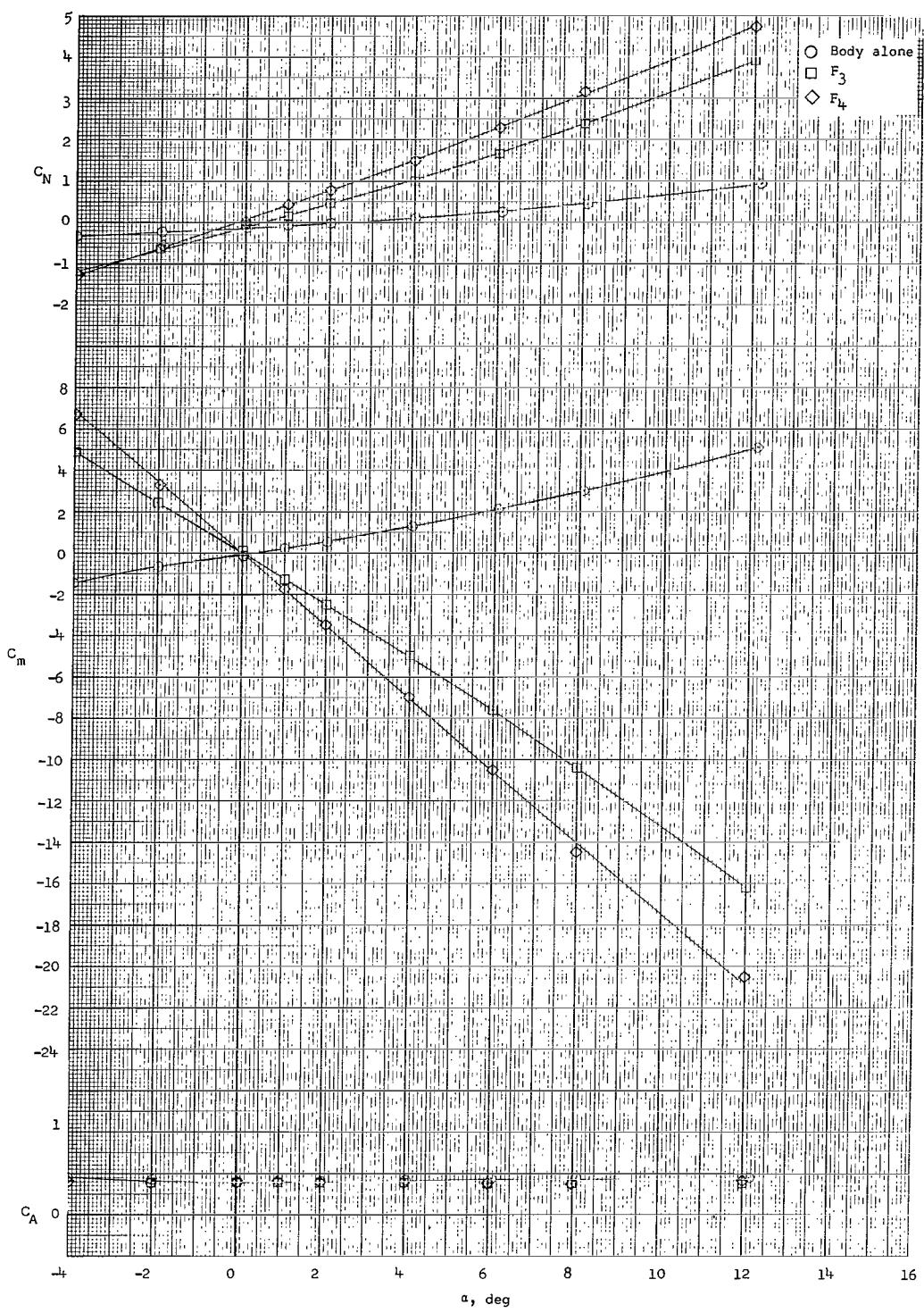
(a) $M_\infty = 0.4$.

Figure 5.- Longitudinal characteristics of model 1 with two fin sizes.
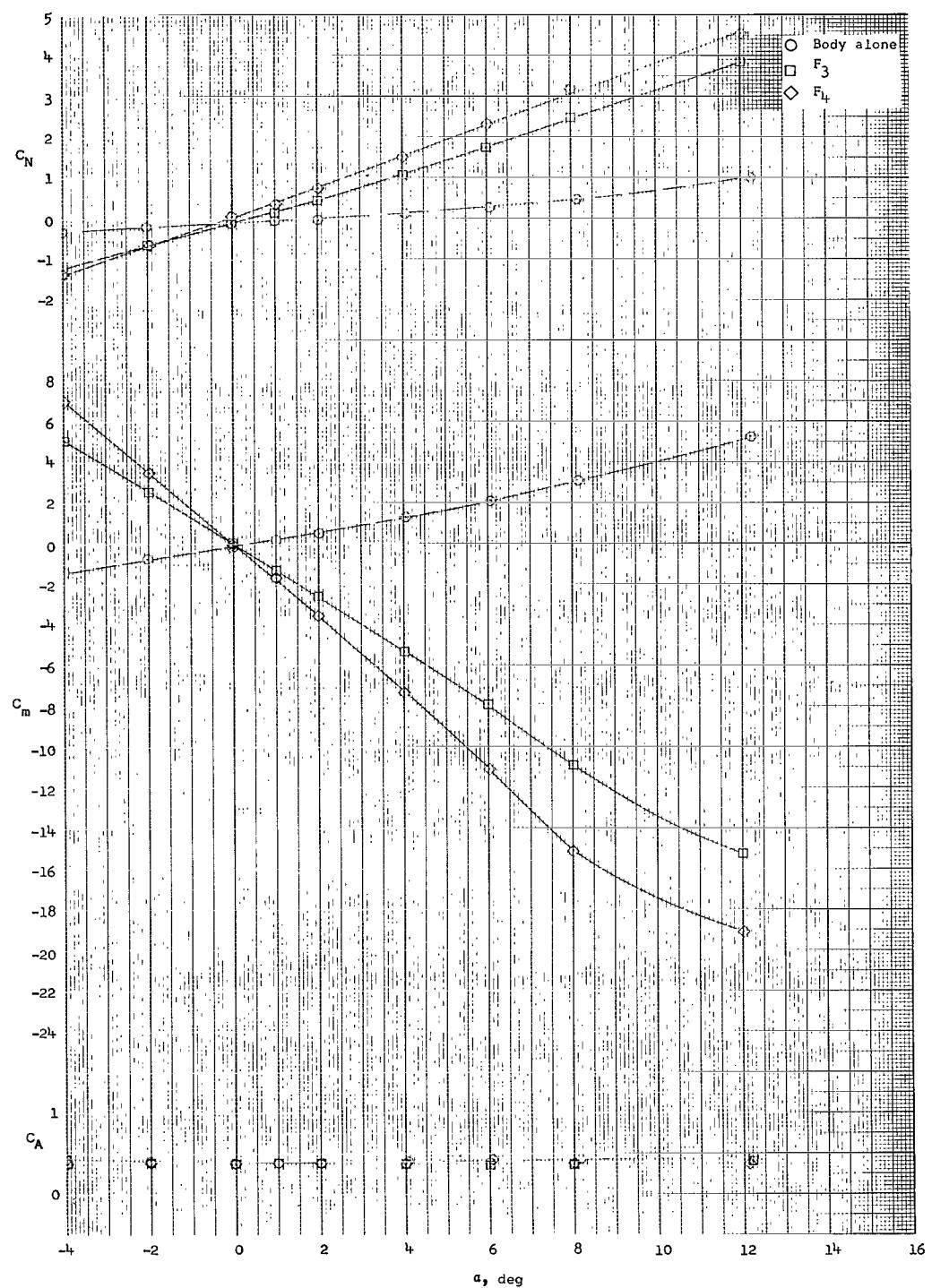
(b) $M_\infty = 0.6$.

Figure 5.- Continued.
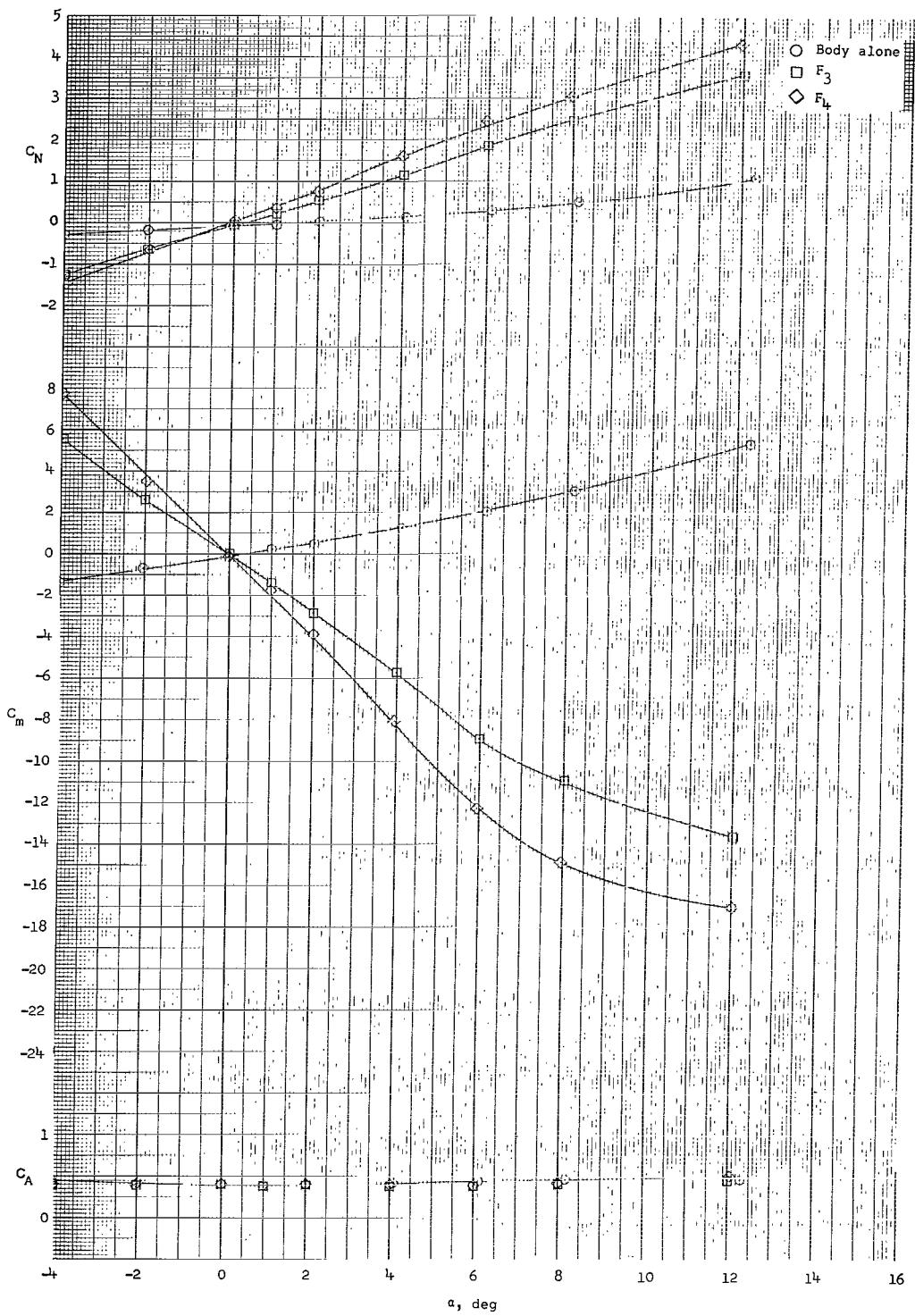
(c) $M_\infty = 0.8$.

Figure 5.- Continued.
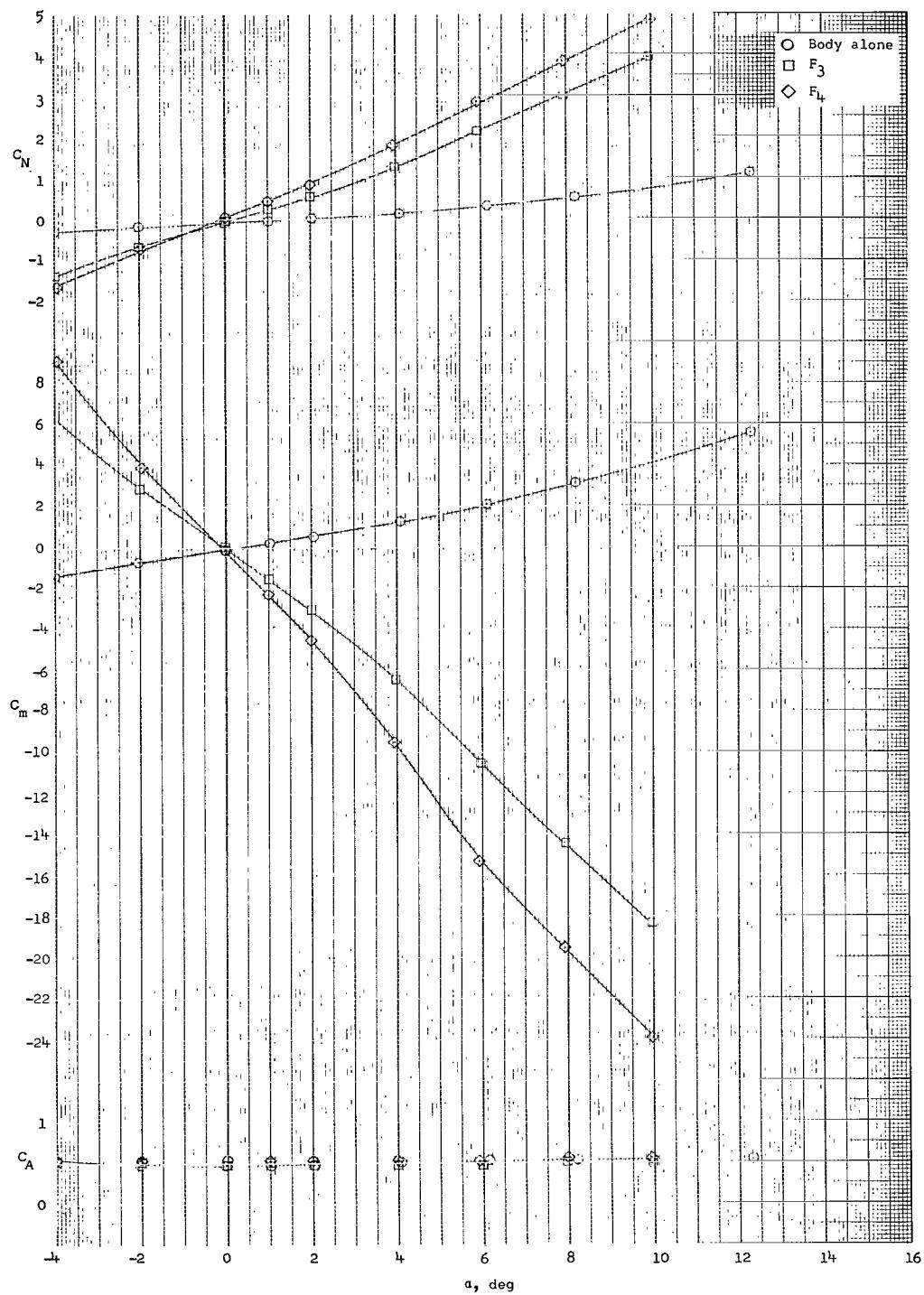
(d) $M_\infty = 0.90$.

Figure 5.- Continued.
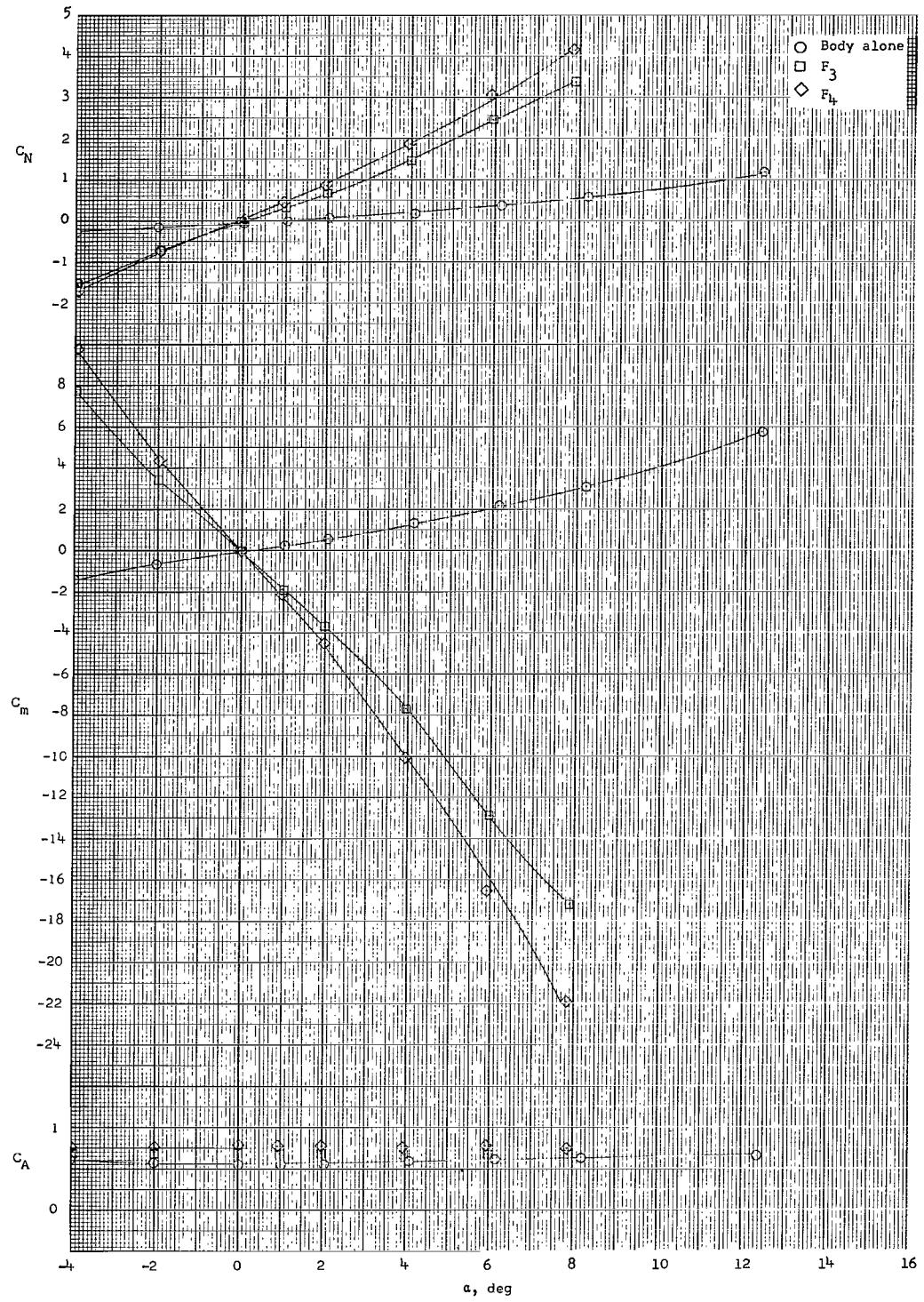
(e) $M_\infty = 0.95$.

Figure 5.- Continued.
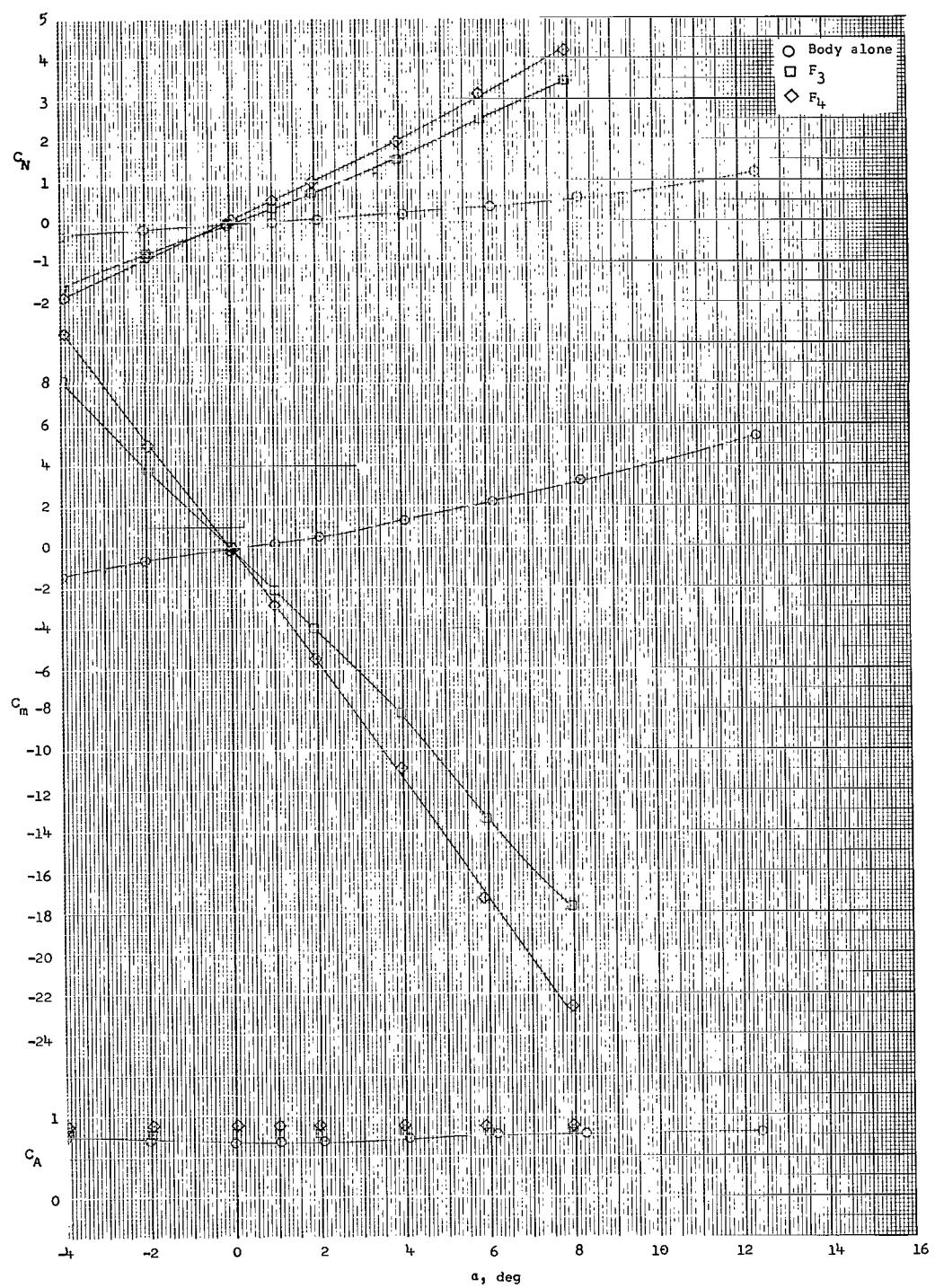
(f) $M_\infty = 1.0$.

Figure 5.- Continued.
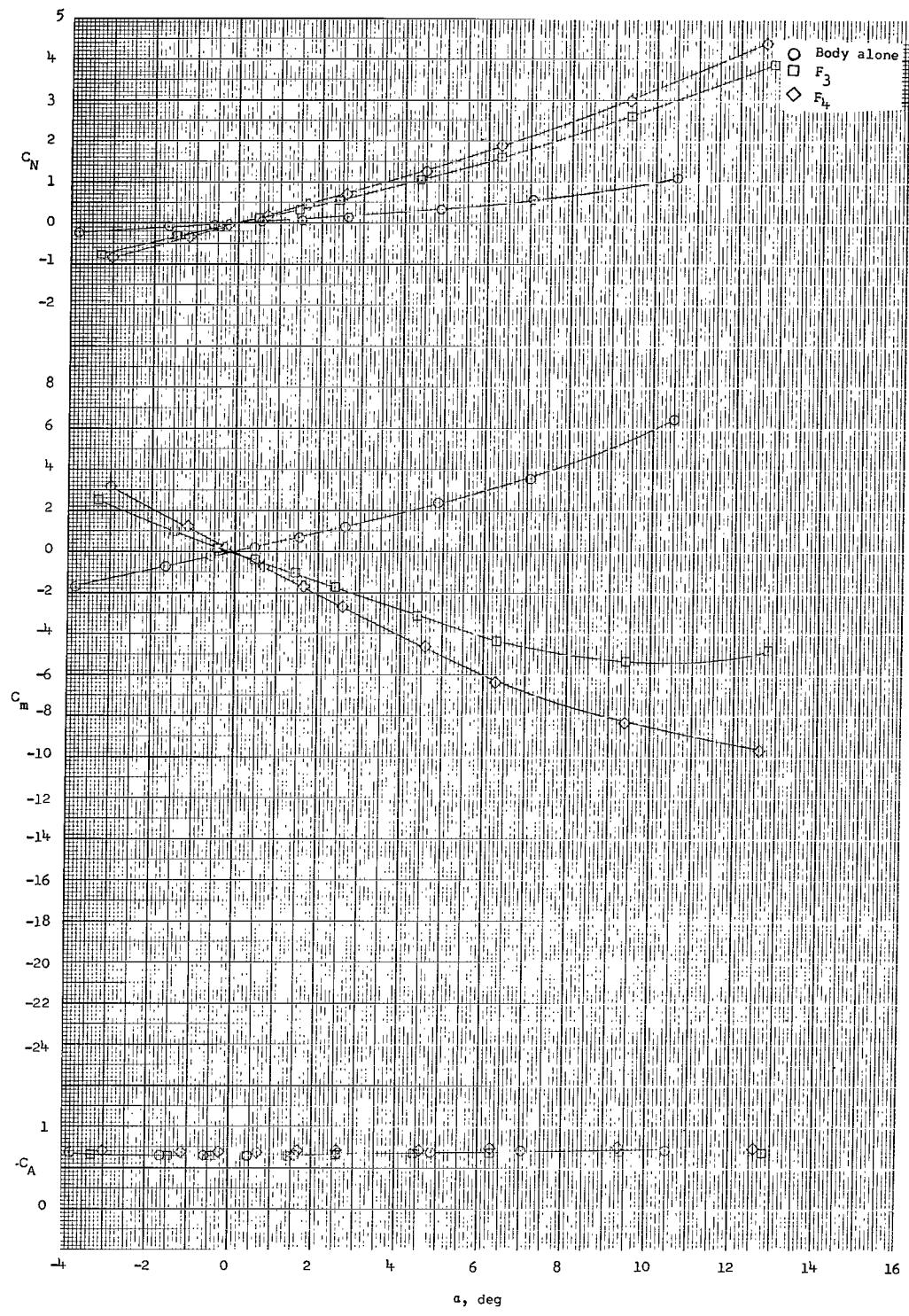
(g) $M_\infty = 2.0$.

Figure 5.- Continued.
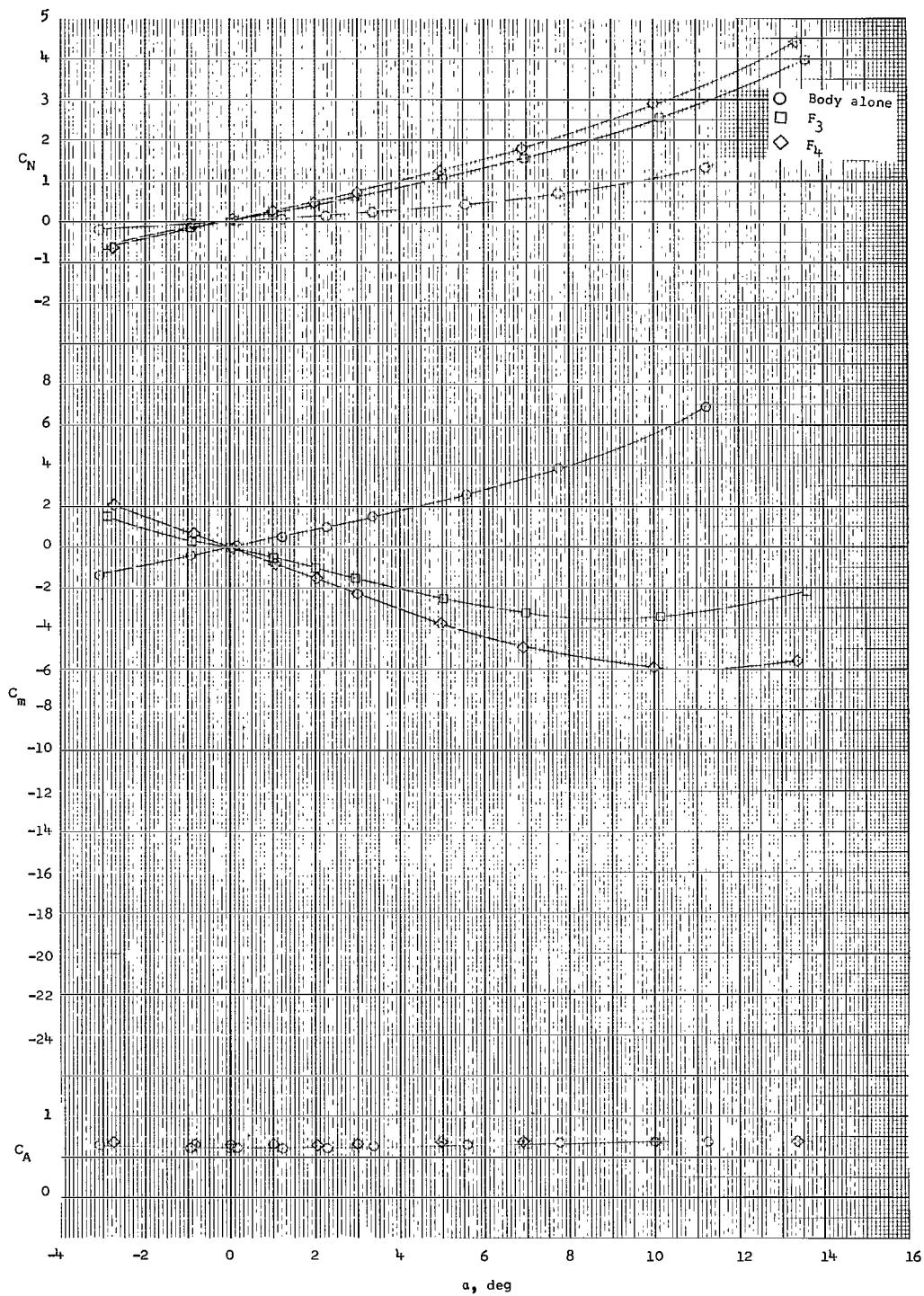
(h) $M_\infty = 2.36$.

Figure 5.- Continued.
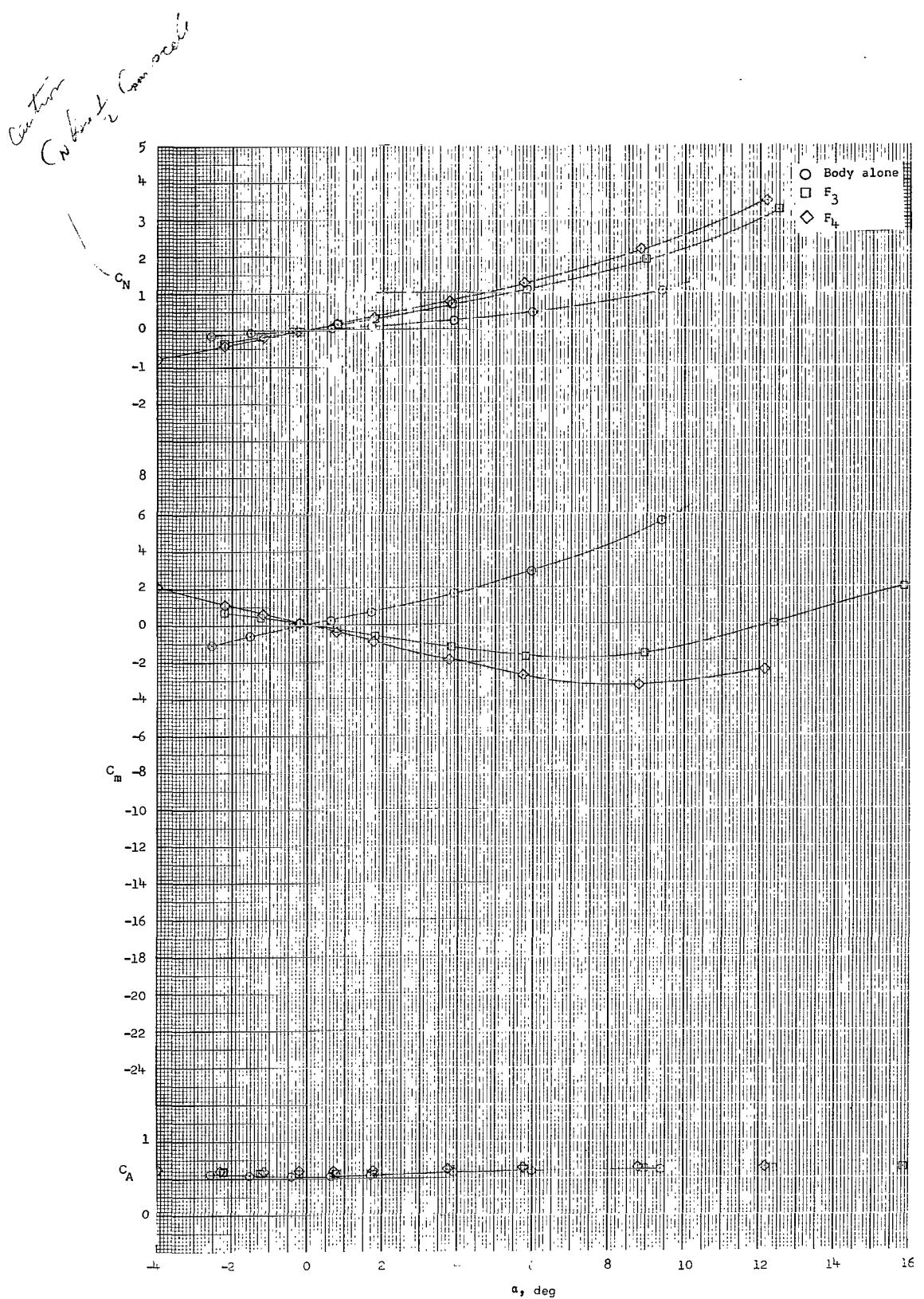
(i) $M_\infty = 2.86$.

Figure 5.- Continued.
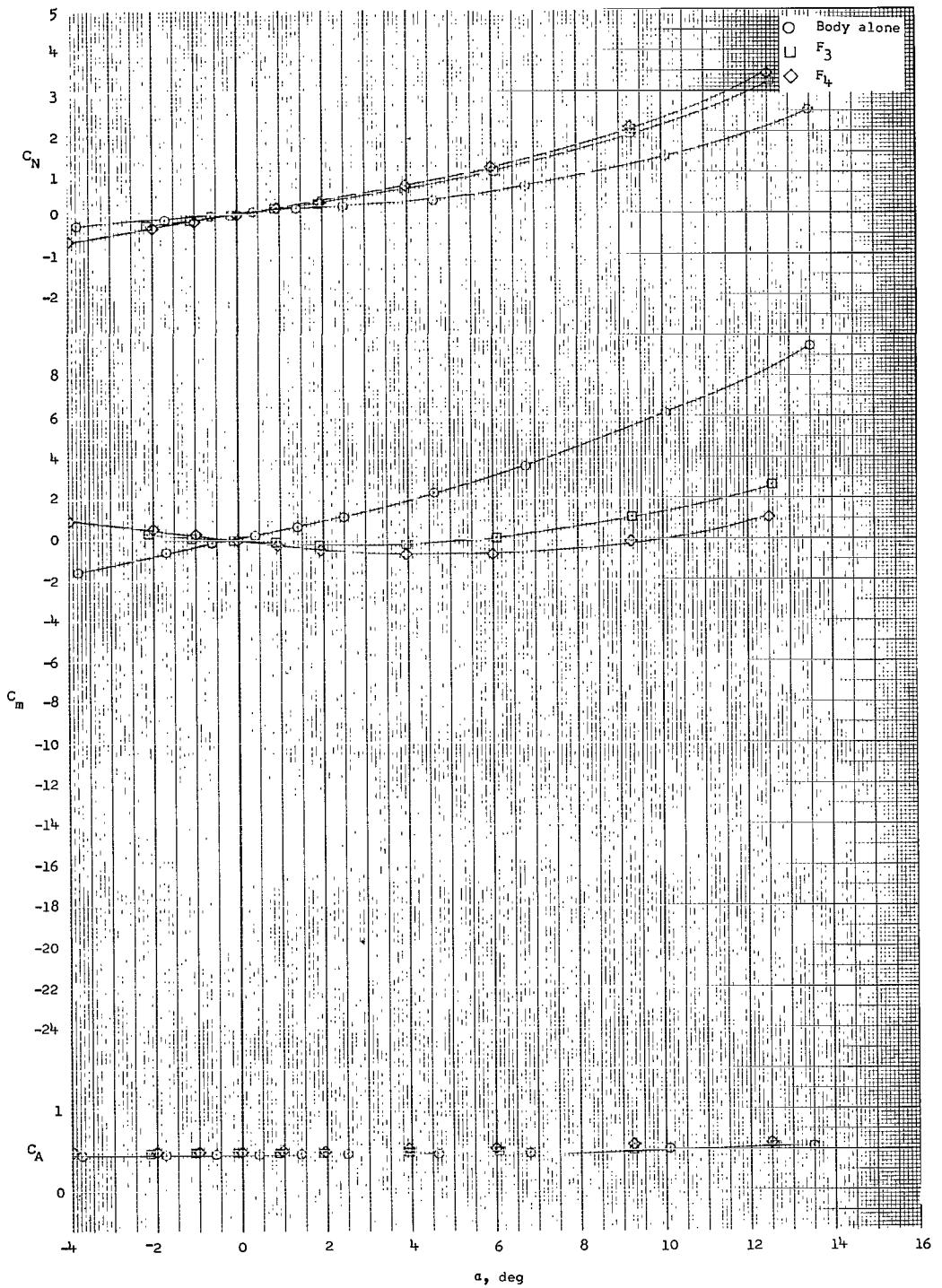
(j) $M_\infty = 3.95.$

Figure 5.- Continued.
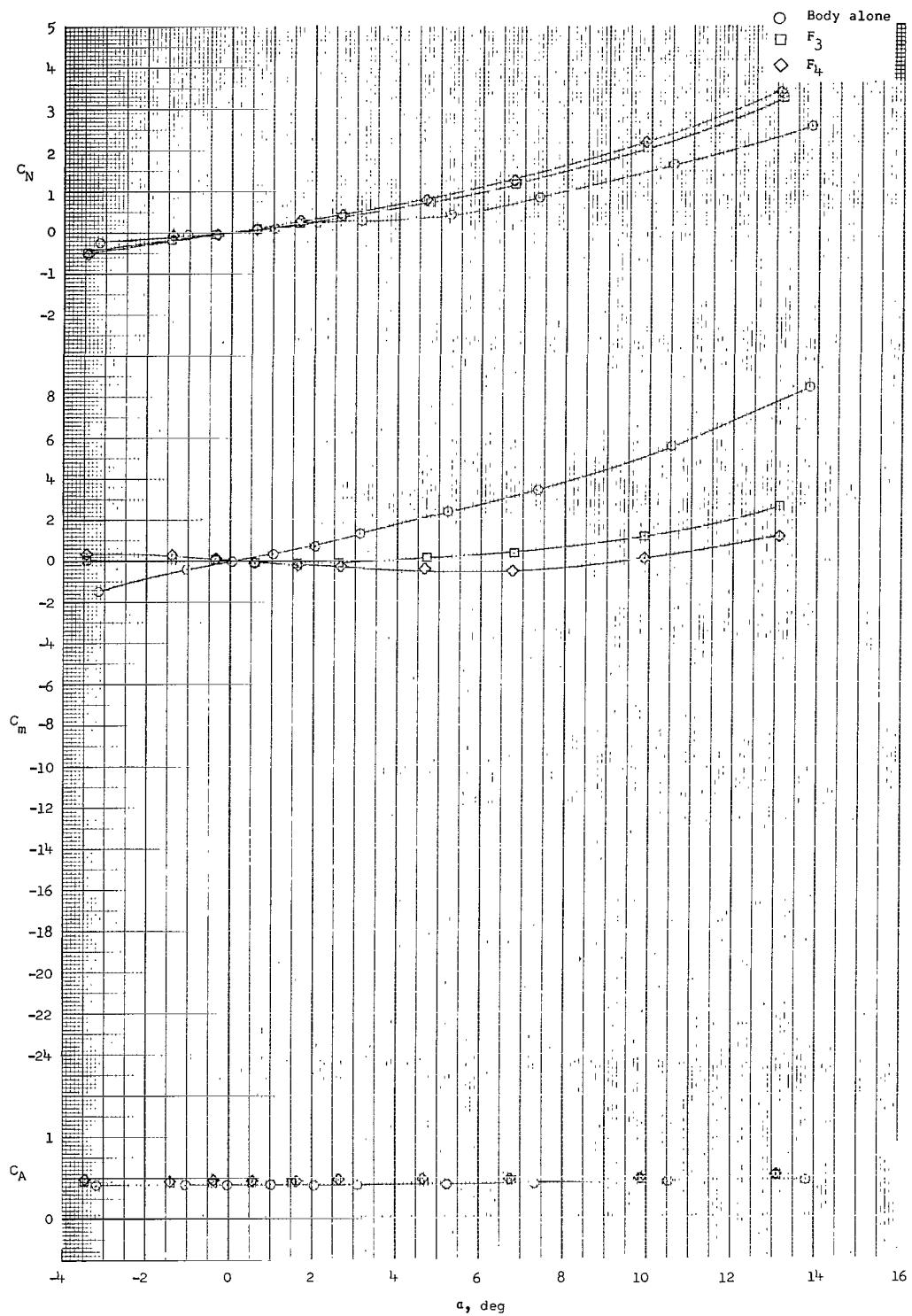
(k) $M_\infty = 4.63$.

Figure 5.- Concluded.
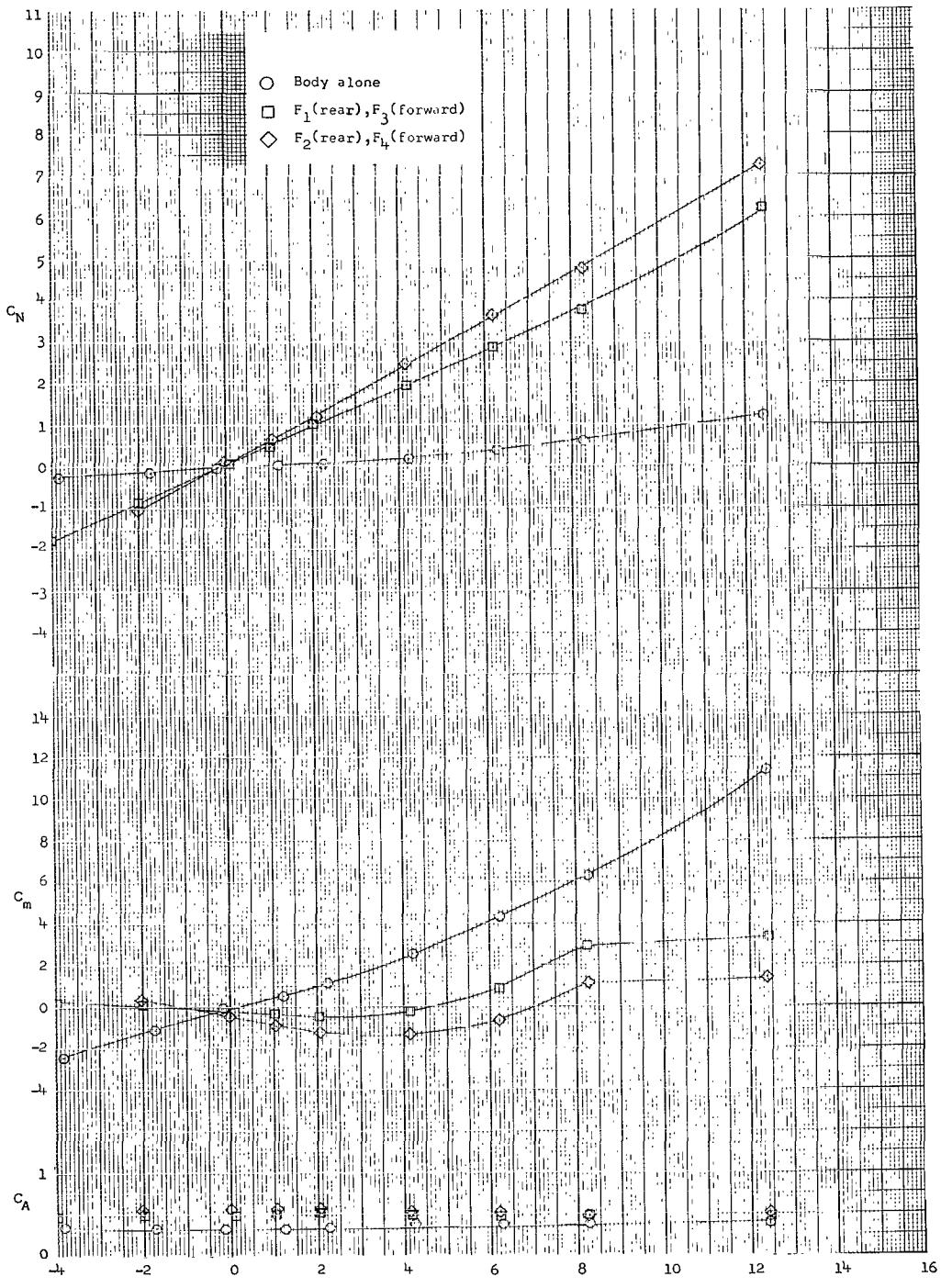
(a) $M_\infty = 0.4$.

Figure 6.- Longitudinal characteristics of model 2 with fin variations.
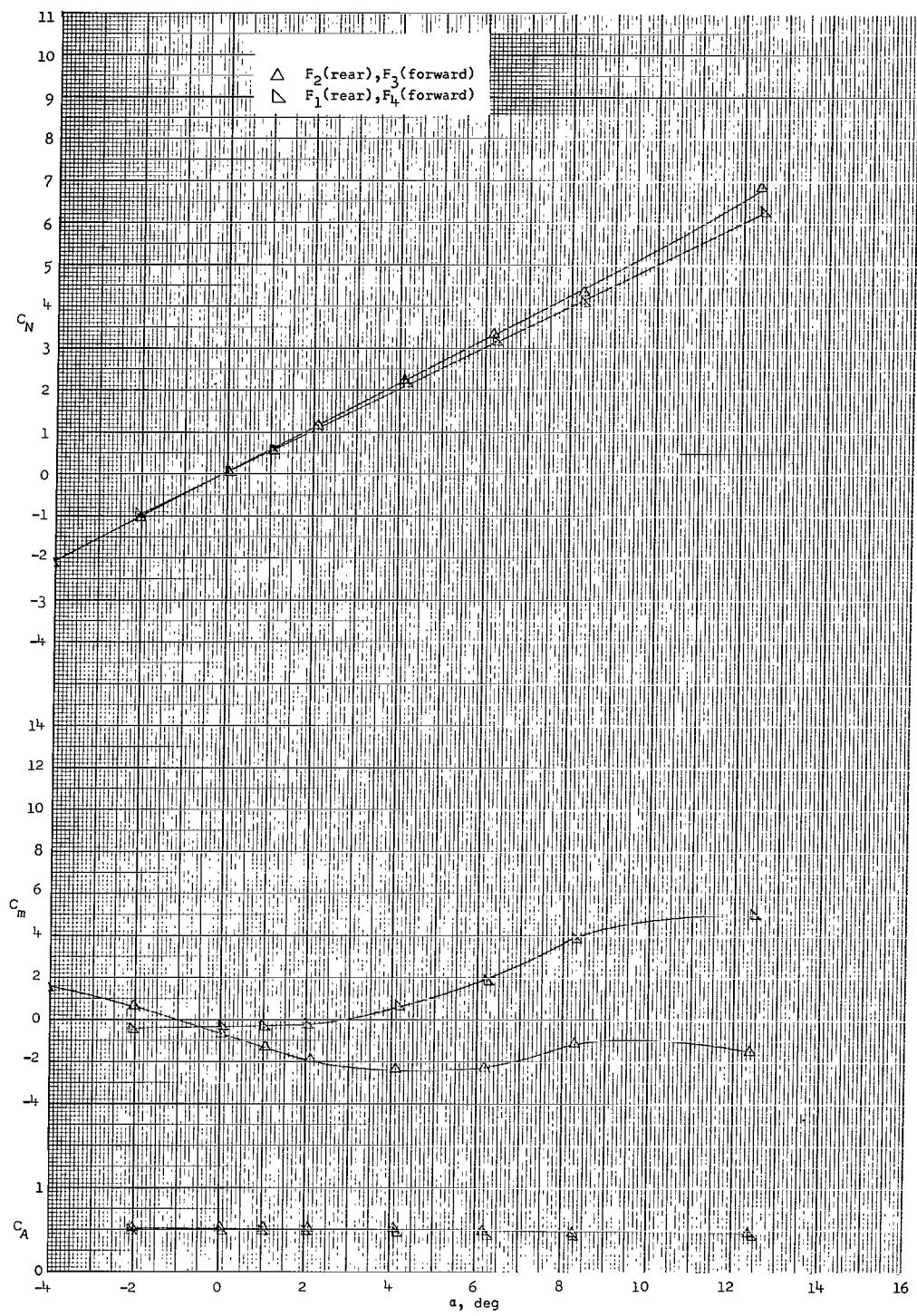
(a) $M_\infty = 0.4$. Concluded.

Figure 6.- Continued.
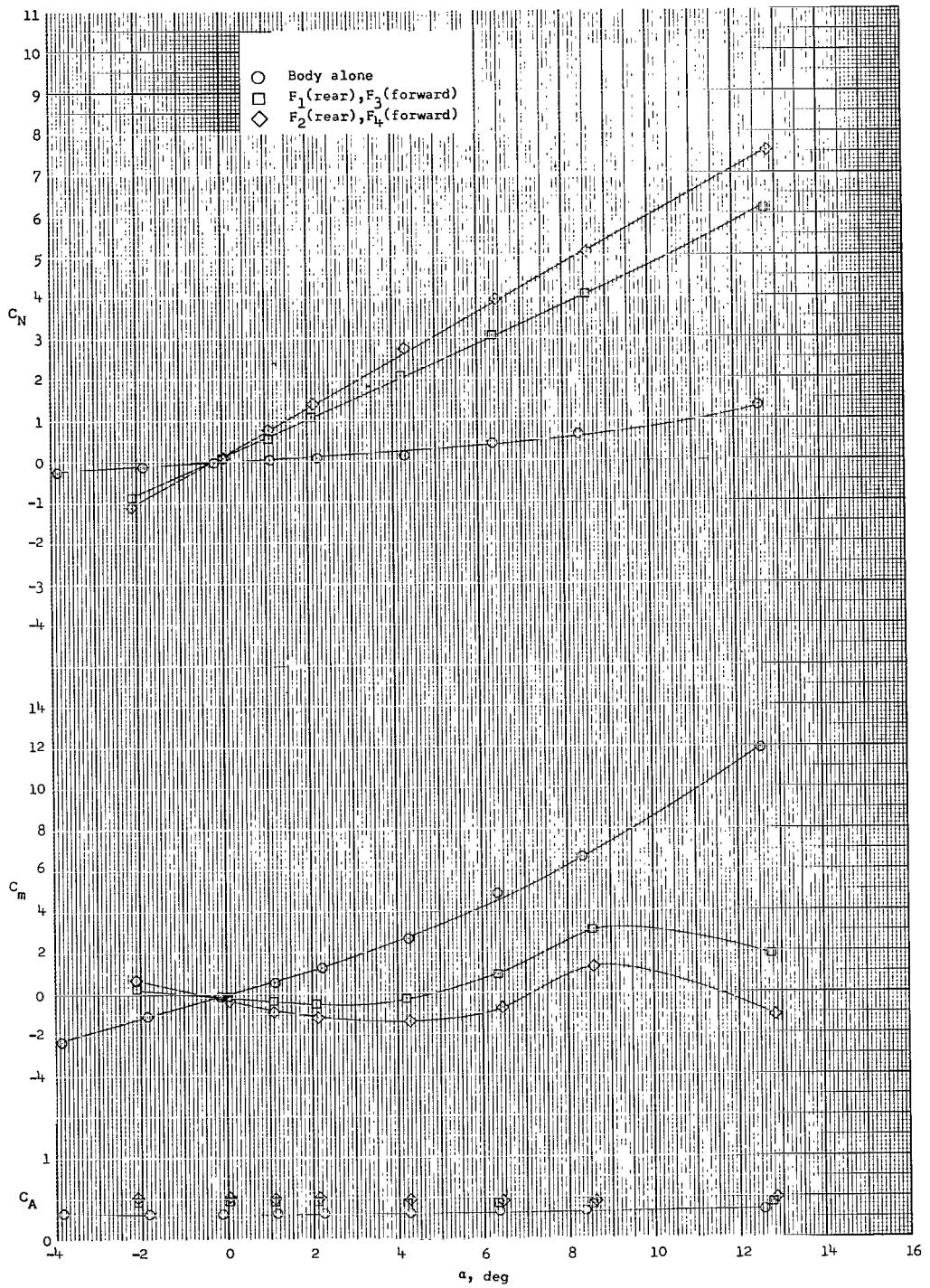
(b) $M_\infty = 0.6$.

Figure 6.- Continued.
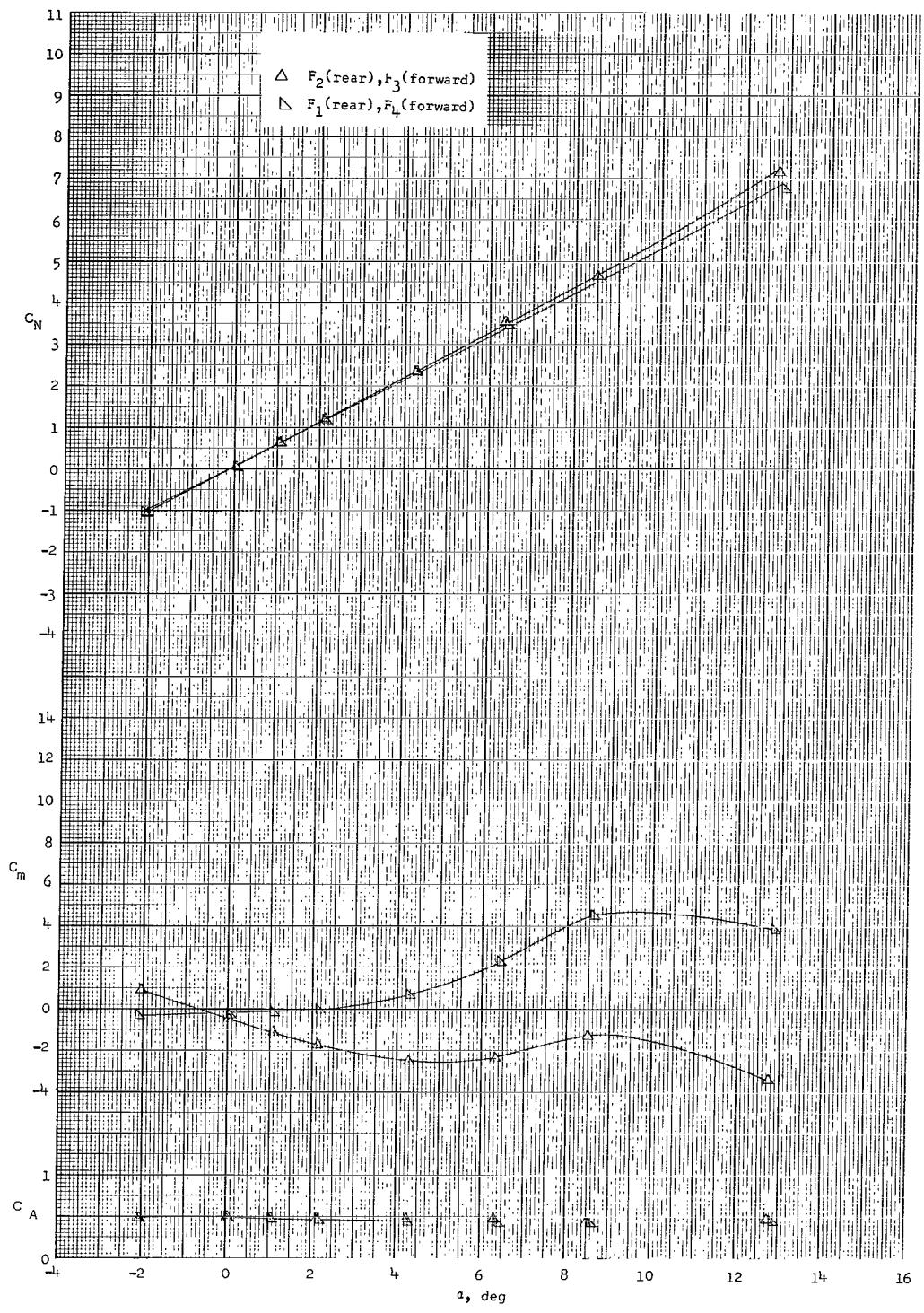
(b) $M_\infty = 0.6$. Concluded.

Figure 6.- Continued.
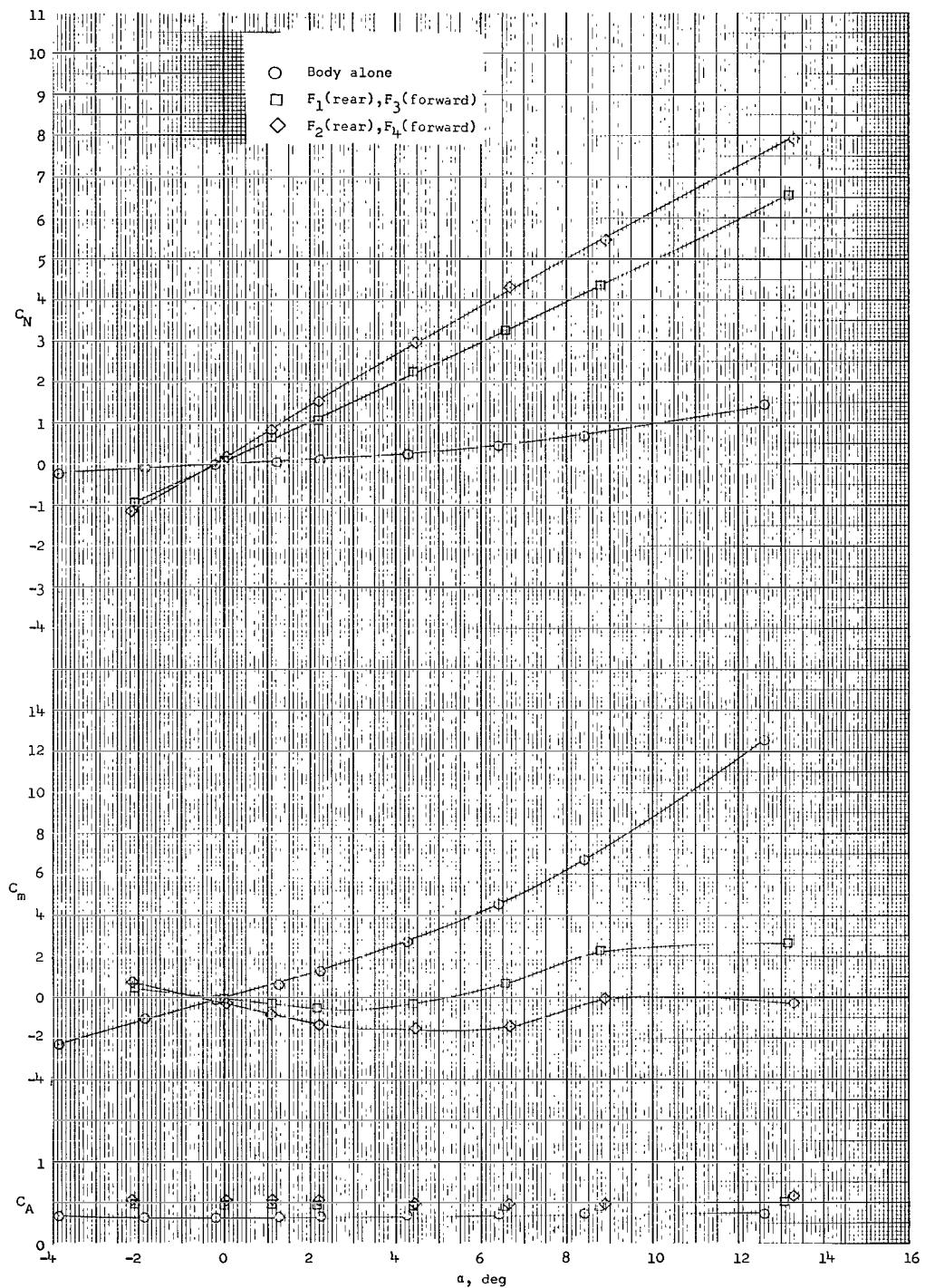
(c) $M_\infty = 0.8$.

Figure 6.- Continued.
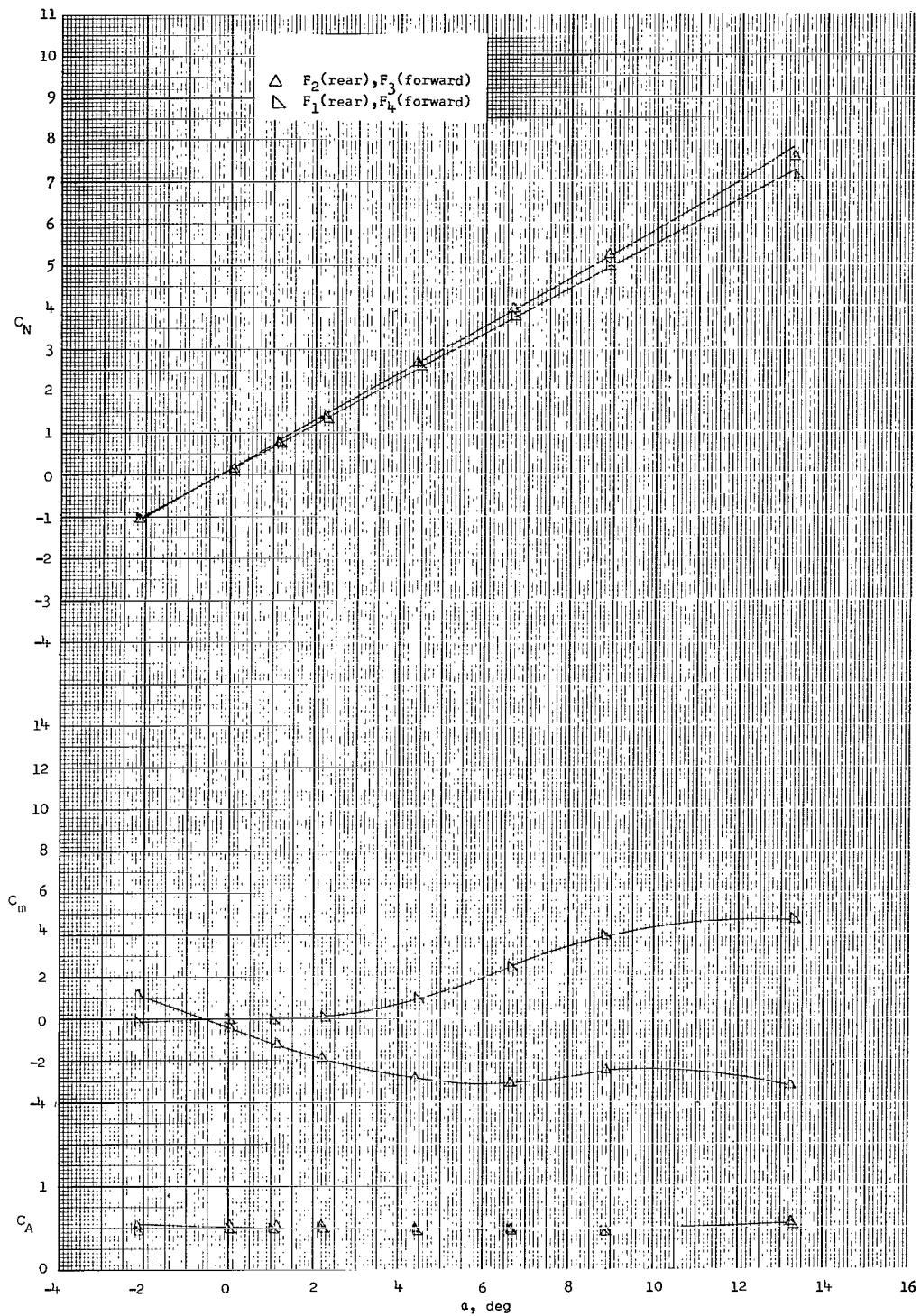
(c) $M_\infty = 0.8$. Concluded.

Figure 6.- Continued.
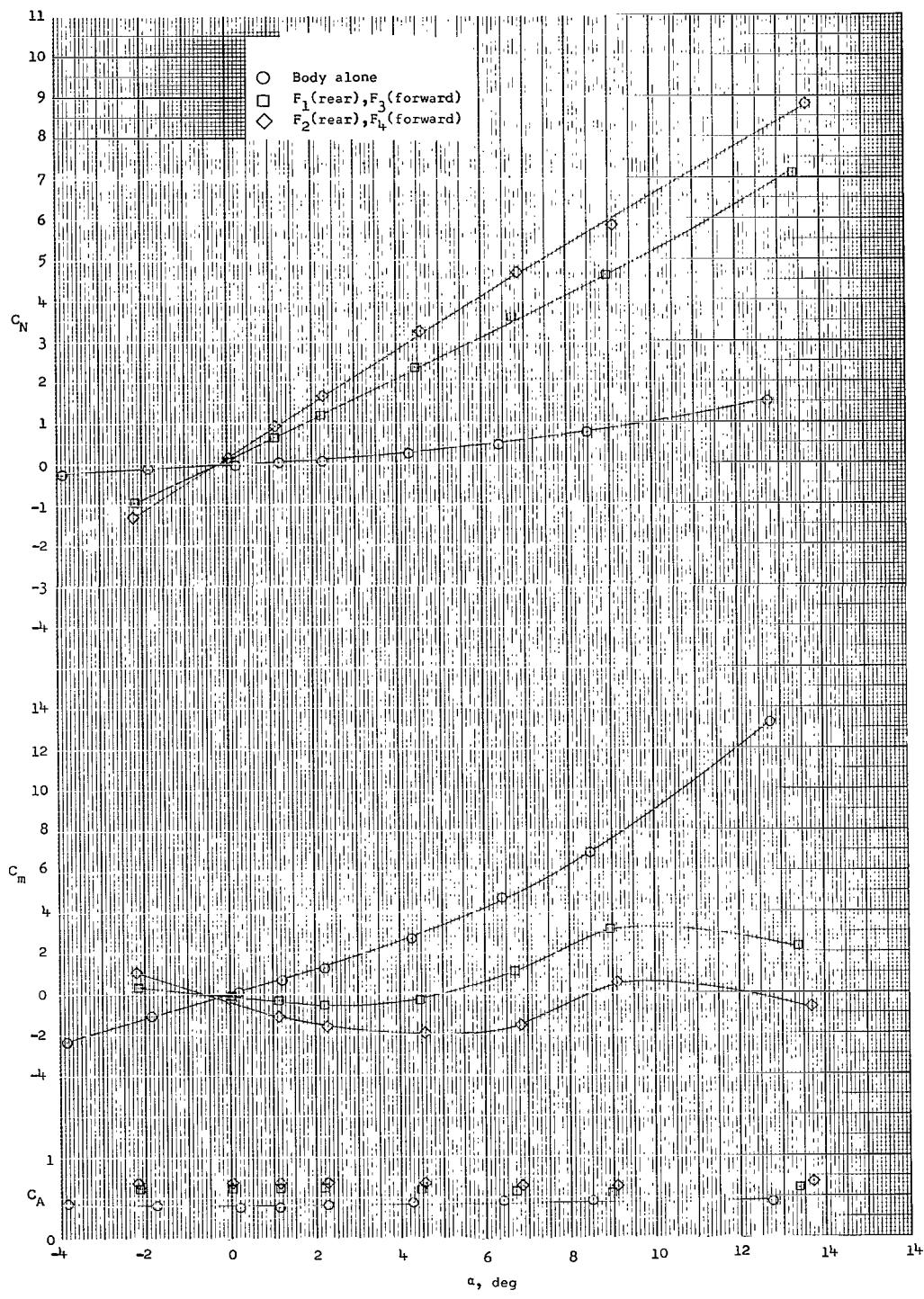
(d) $M_{\infty} = 0.9$.

Figure 6.- Continued.
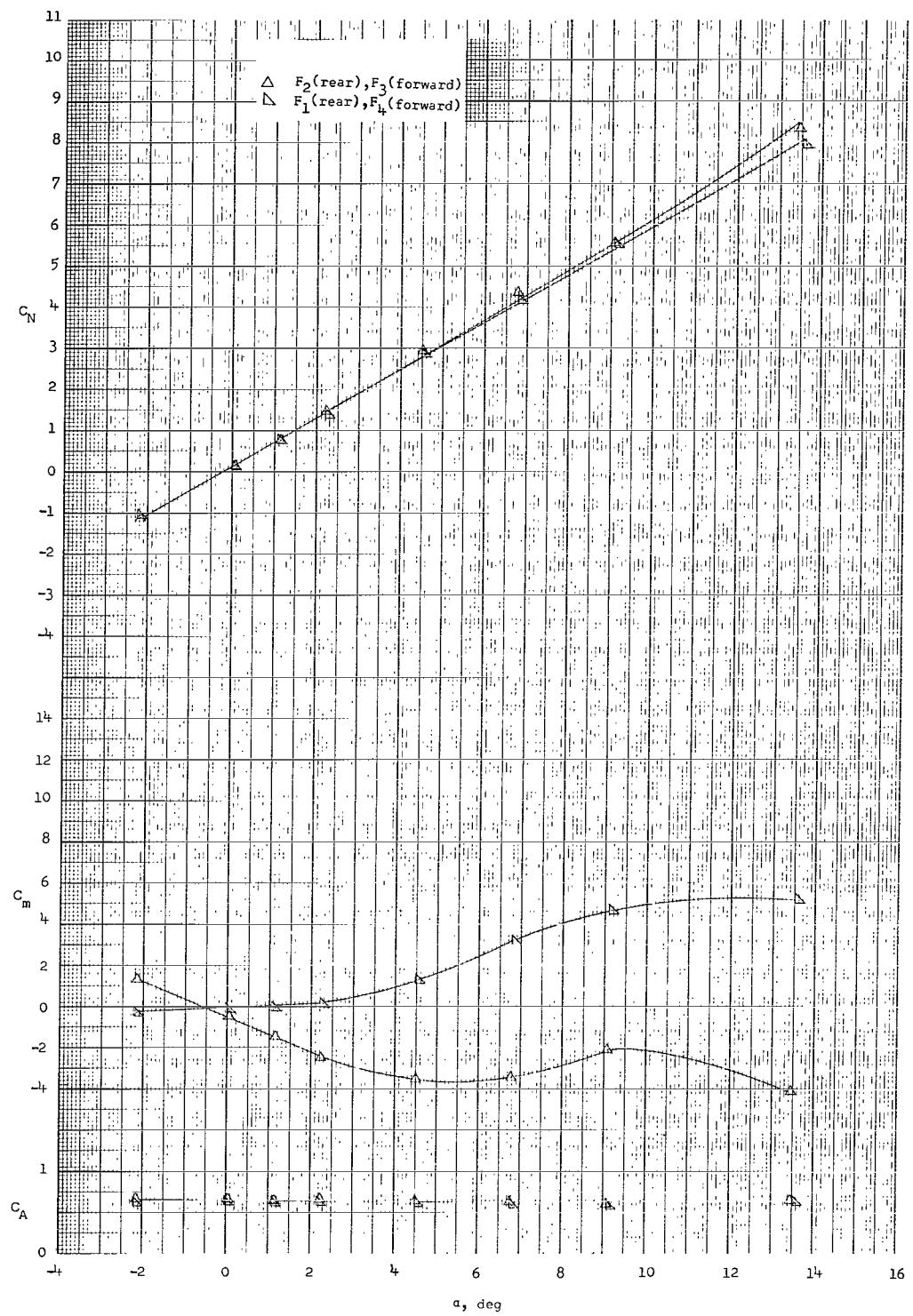
(d) $M_\infty = 0.9$. Concluded.

Figure 6.- Continued.
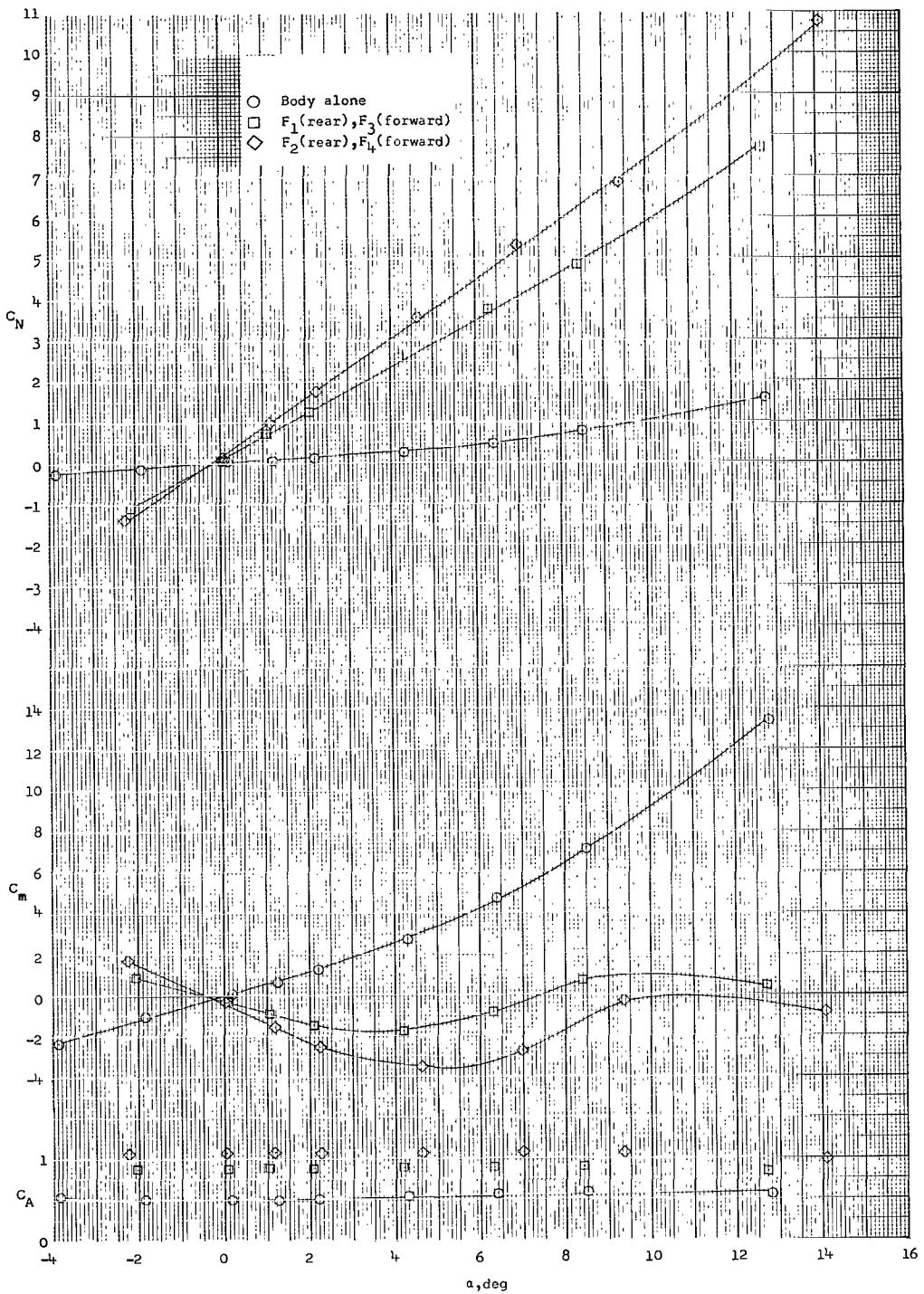
(e) $M_\infty = 0.95$.

Figure 6.- Continued.
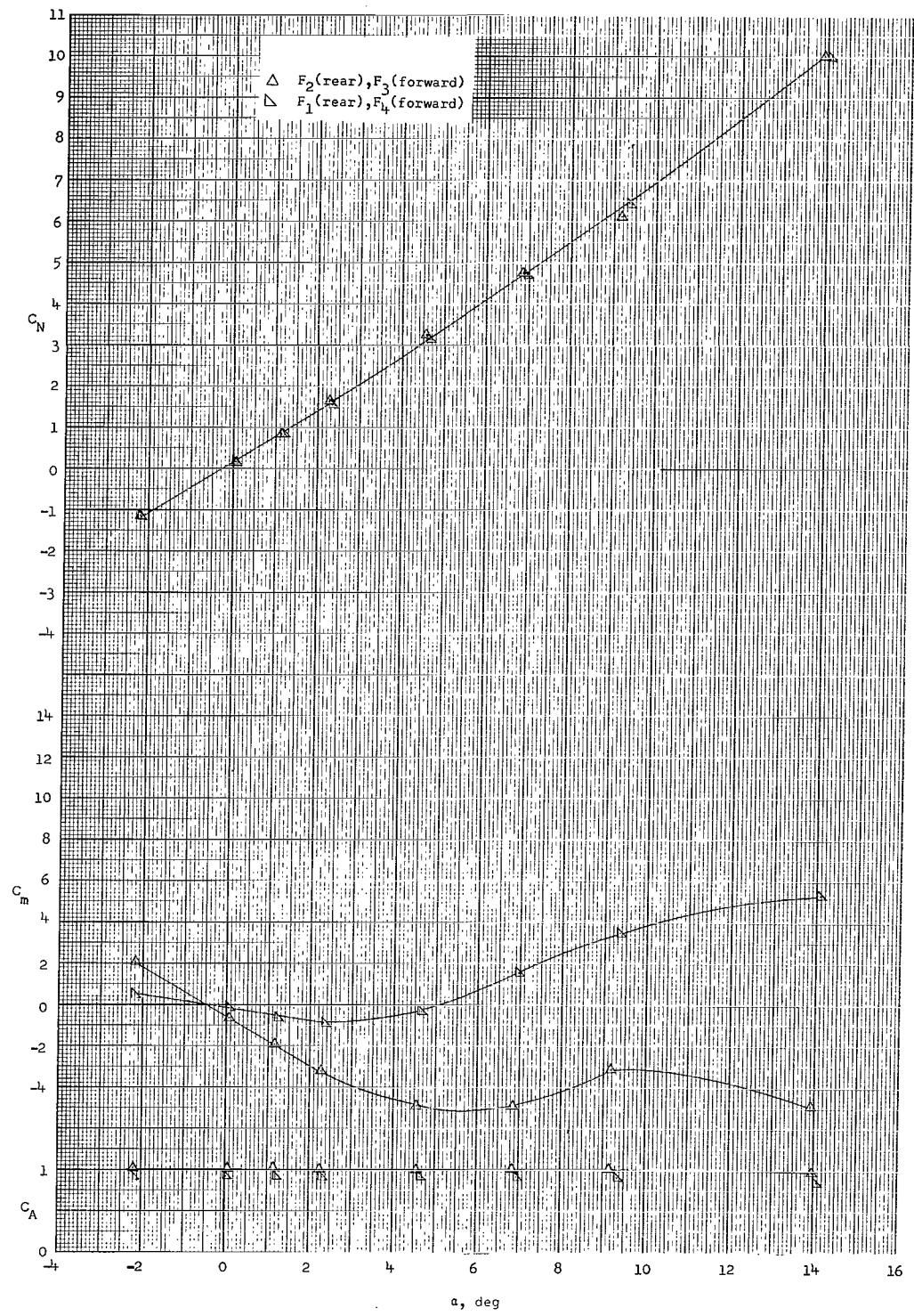
(e) $M_\infty = 0.95$. Concluded.

Figure 6.- Continued.
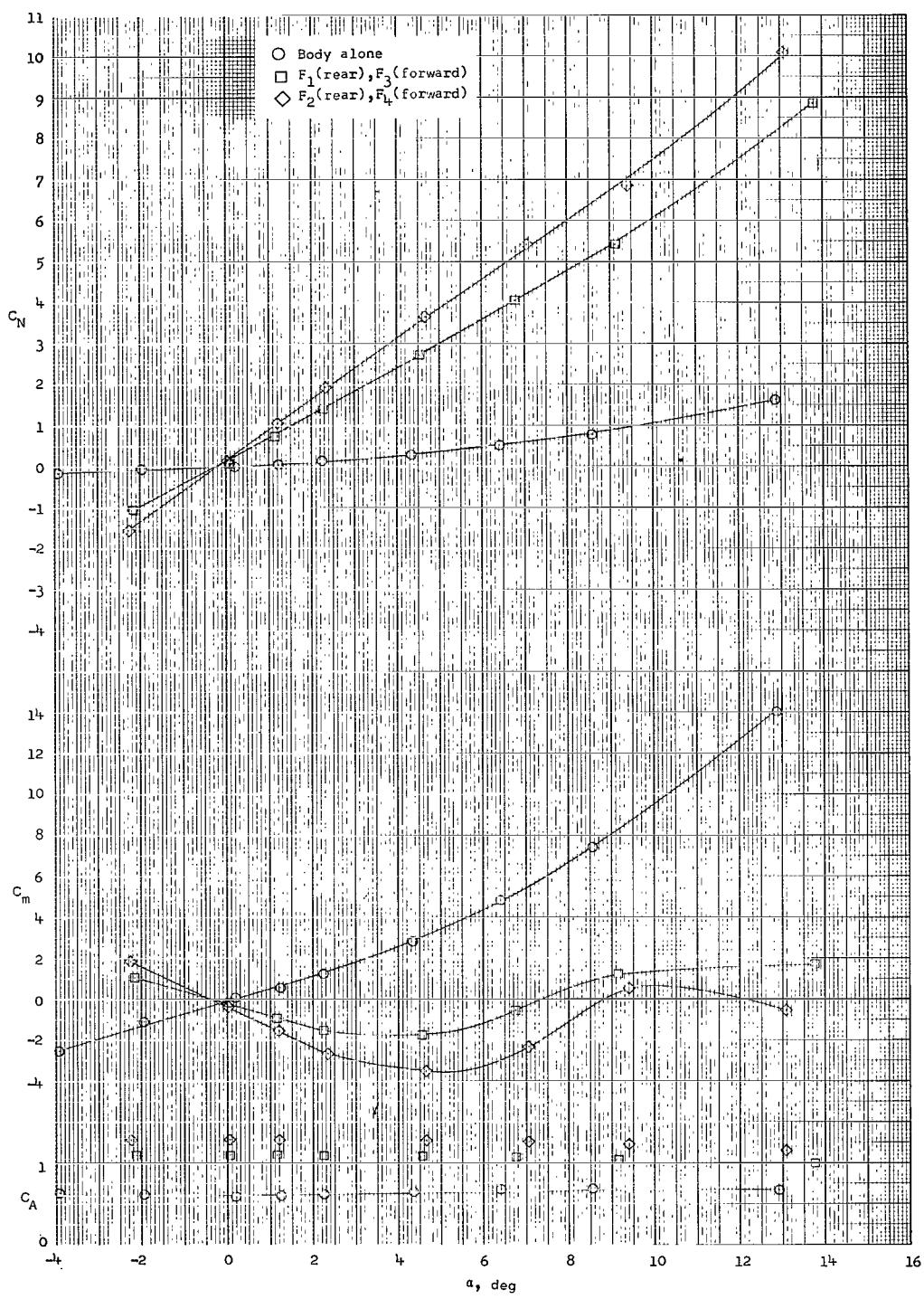
(f) $M_\infty = 1.0$.

Figure 6.- Continued.
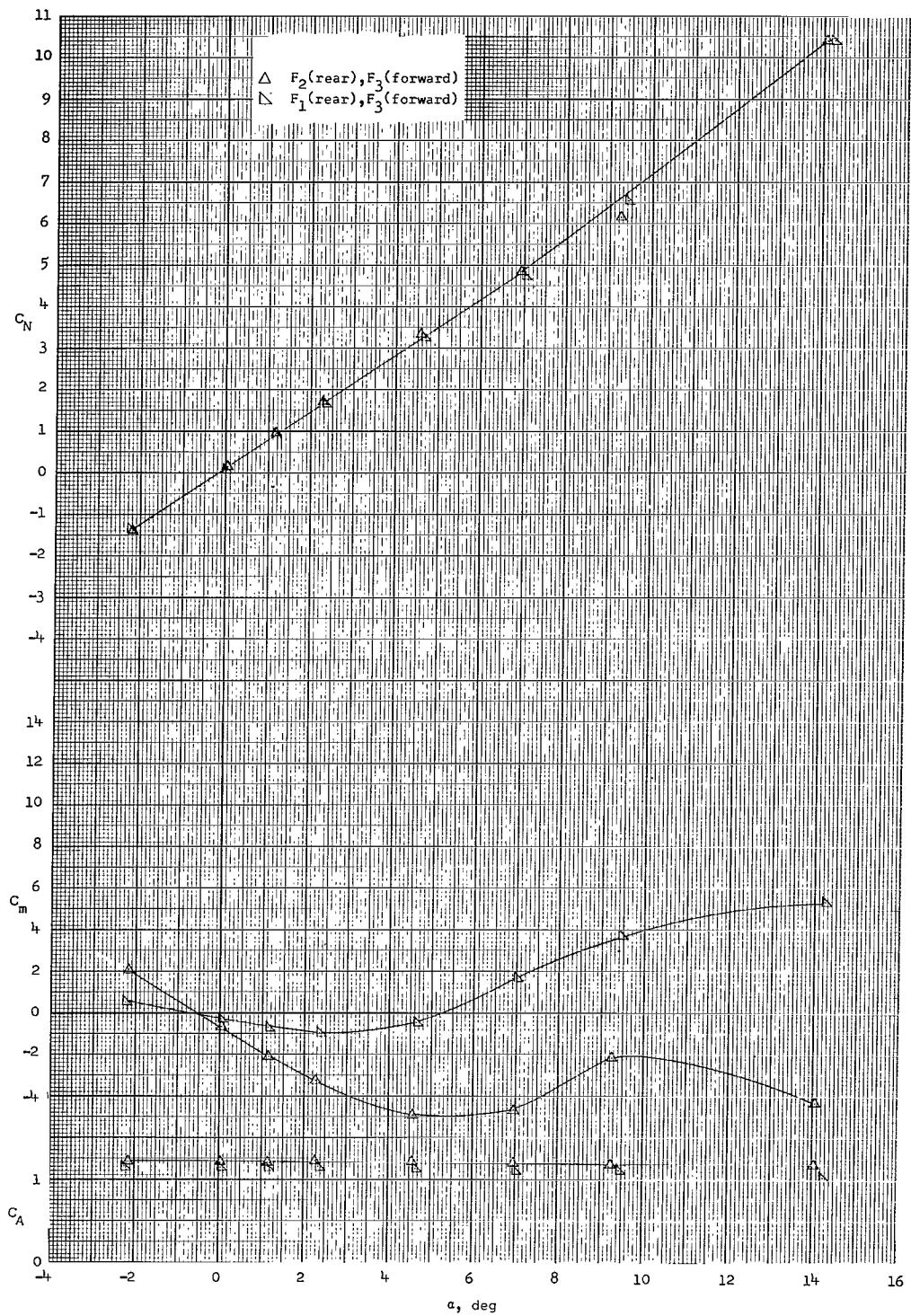
(f) $M_\infty = 1.0$. Concluded.

Figure 6.- Concluded.
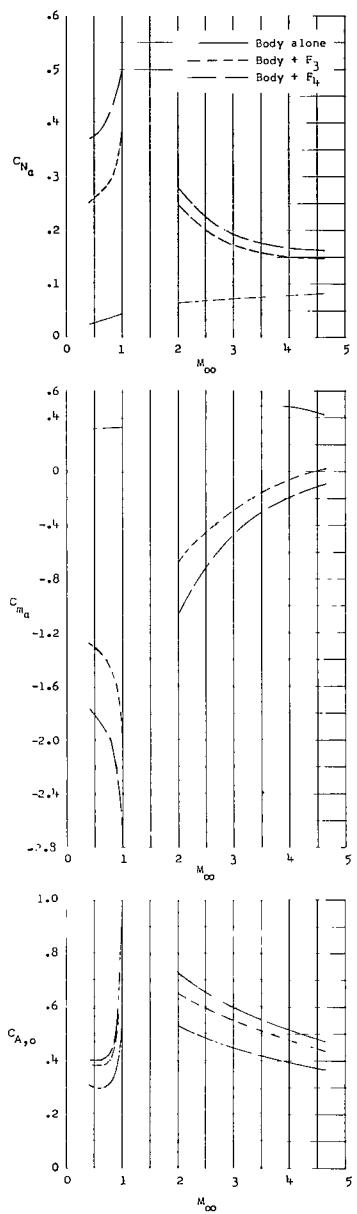
(a) Model 1.

Figure 7.- Variation of longitudinal aerodynamic parameters with Mach number. $\alpha = 0^0$.
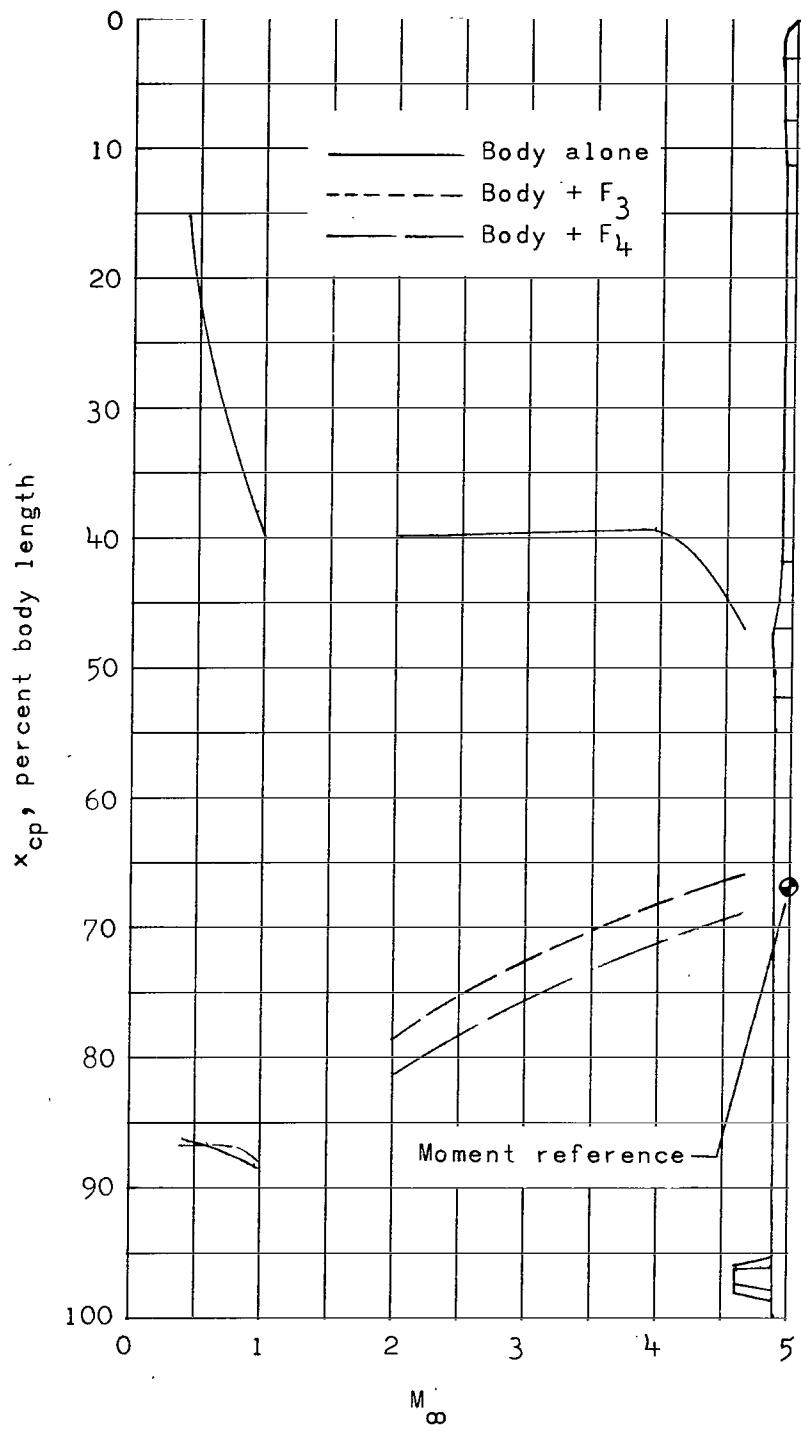
(b) Model 1.

Figure 7.- Continued.
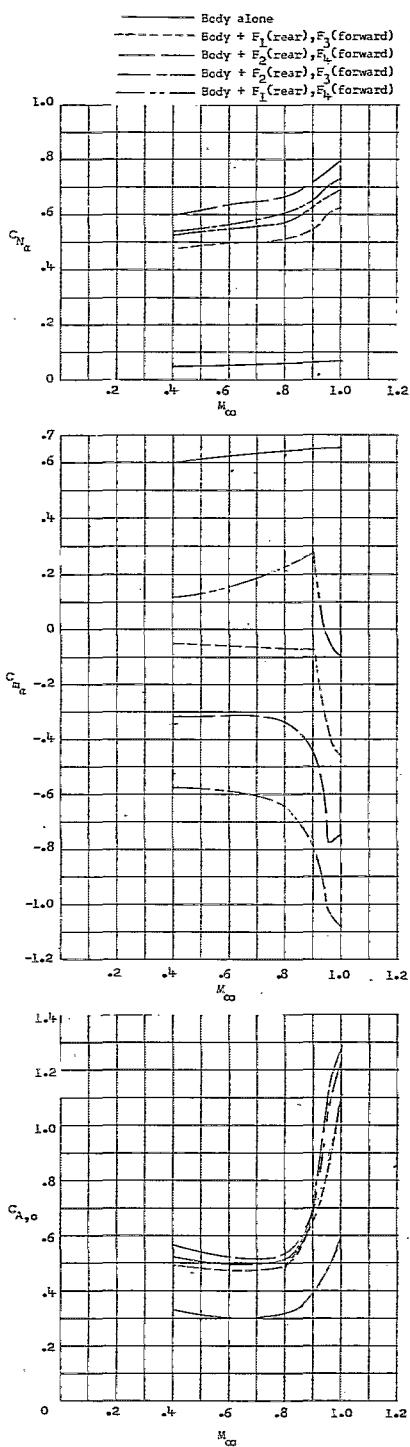
(c) Model 2.

Figure 7.- Continued.
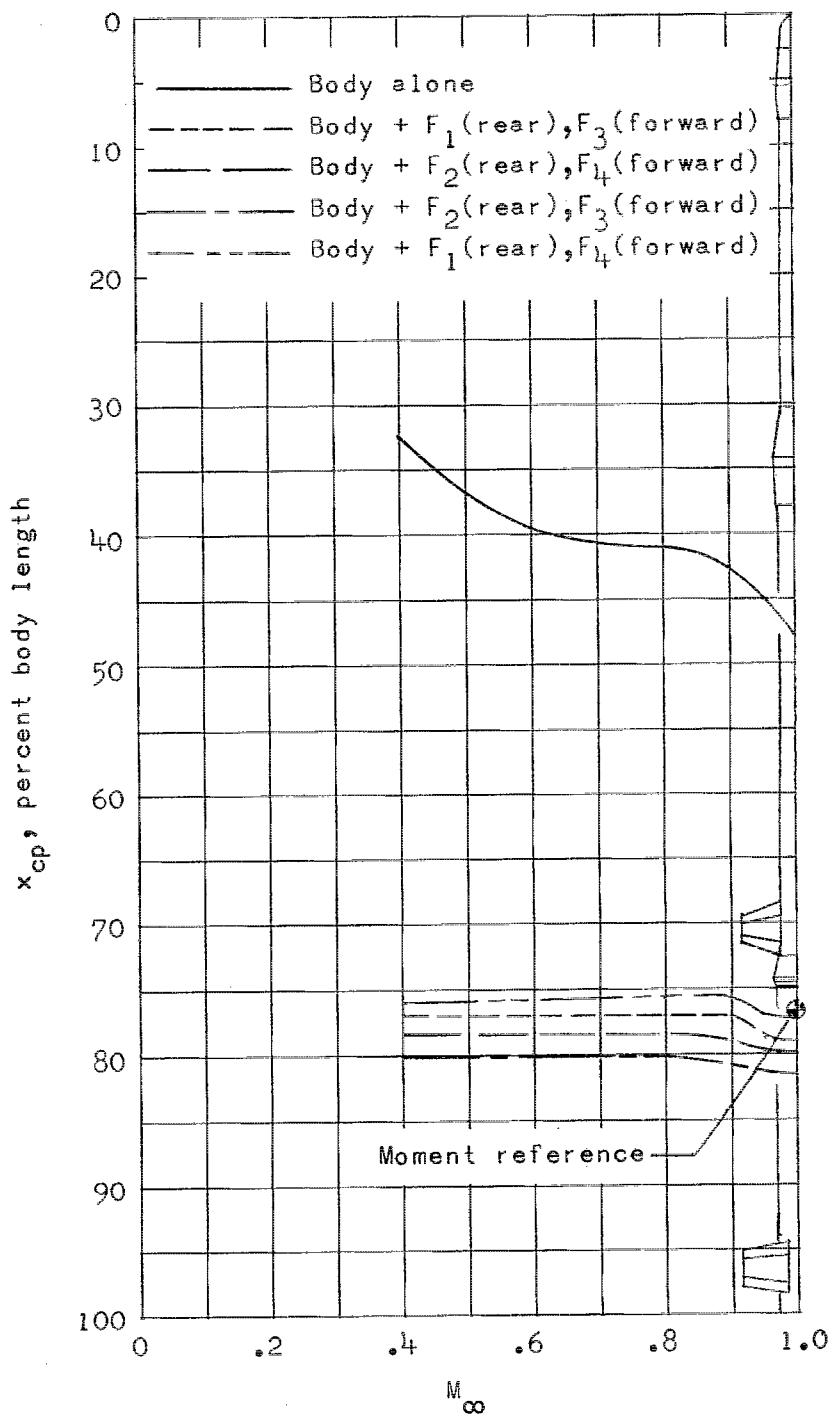
(d) Model 2.

Figure 7.- Concluded.
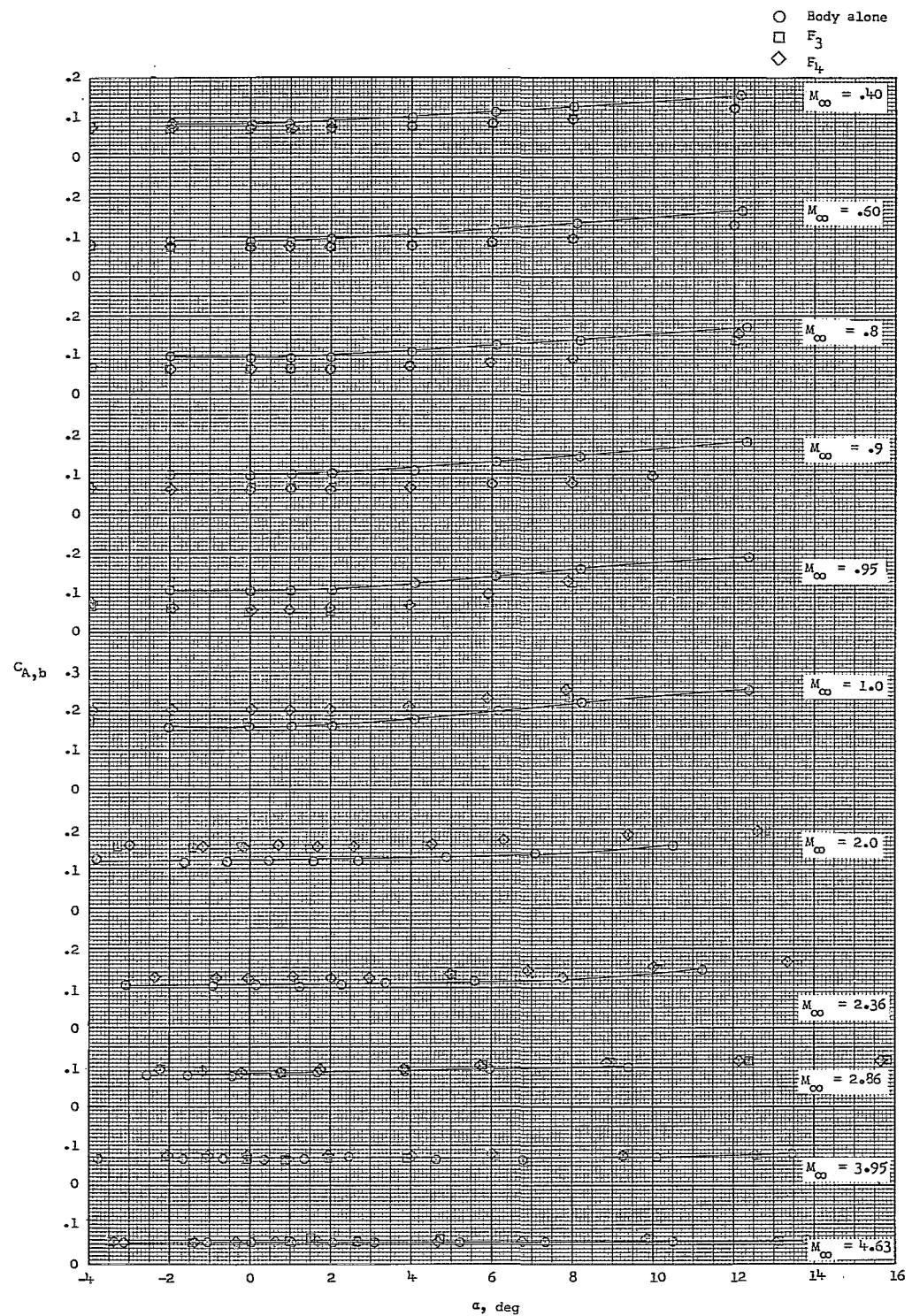
(a) Model 1.

Figure 8.- Base axial-force coefficient as a function of angle of attack for the various model configurations and test Mach numbers.
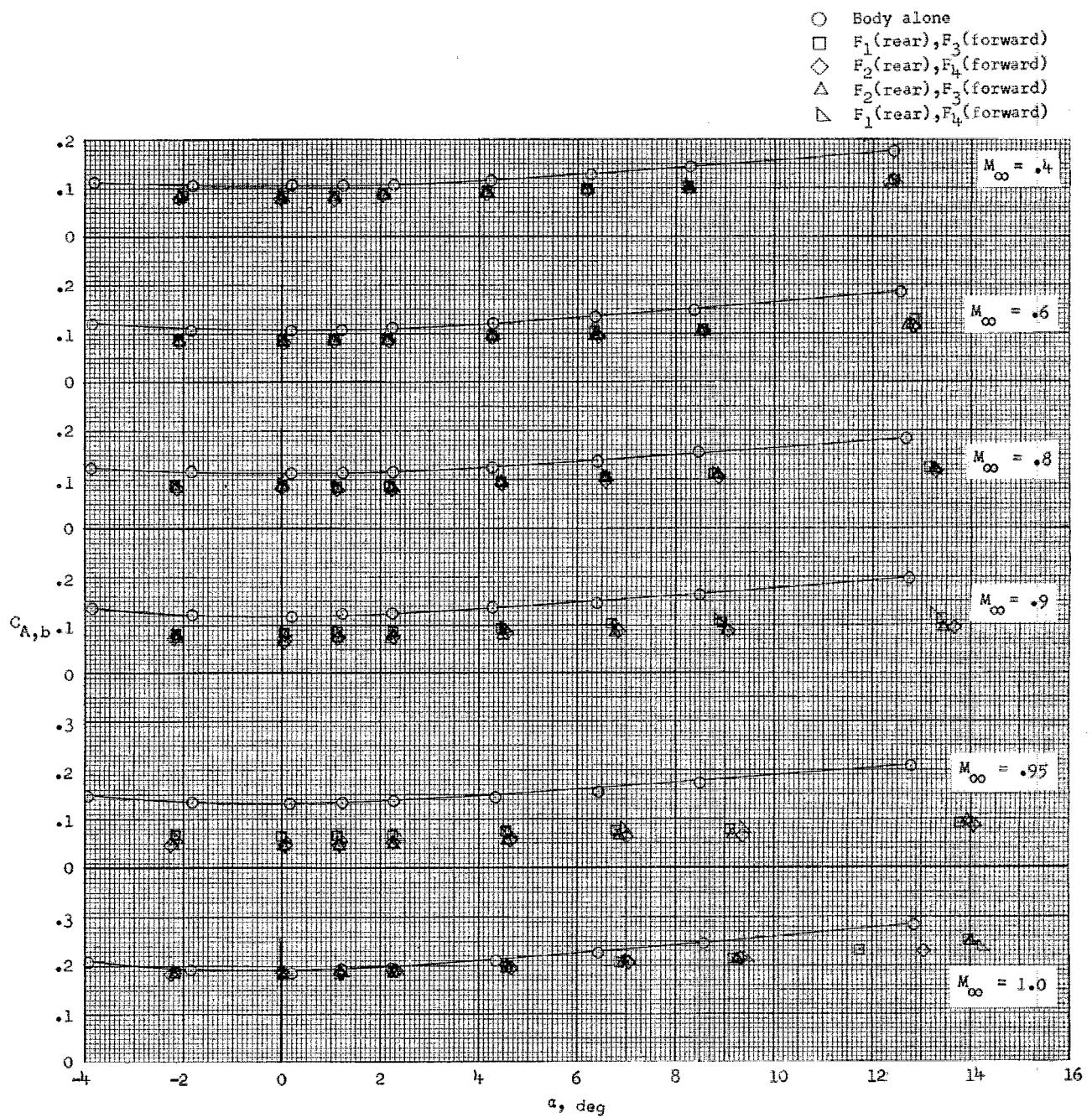
(b) Model 2.

Figure 8.- Concluded.
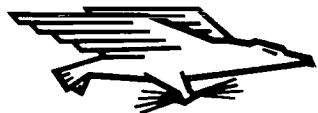
POSTMASTER: If Undeliverable (Section 158
Postal Manual) Do Not Return

*"The aeronautical and space activities of the United States shall be
conducted so as to contribute . . . to the expansion of human knowl-
edge of phenomena in the atmosphere and space. The Administration
shall provide for the widest practicable and appropriate dissemination
of information concerning its activities and the results thereof."*

— NATIONAL AERONAUTICS AND SPACE ACT OF 1958

NASA SCIENTIFIC AND TECHNICAL PUBLICATIONS

TECHNICAL REPORTS: Scientific and
technical information considered important,
complete, and a lasting contribution to existing
knowledge.

TECHNICAL NOTES: Information less broad
in scope but nevertheless of importance as a
contribution to existing knowledge.

TECHNICAL MEMORANDUMS:
Information receiving limited distribution
because of preliminary data, security classifica-
tion, or other reasons.

CONTRACTOR REPORTS: Scientific and
technical information generated under a NASA
contract or grant and considered an important
contribution to existing knowledge.

TECHNICAL TRANSLATIONS: Information
published in a foreign language considered
to merit NASA distribution in English.

SPECIAL PUBLICATIONS: Information
derived from or of value to NASA activities.
Publications include conference proceedings,
monographs, data compilations, handbooks,
sourcebooks, and special bibliographies.

**TECHNOLOGY UTILIZATION
PUBLICATIONS:** Information on technology
used by NASA that may be of particular
interest in commercial and other non-aerospace
applications. Publications include Tech Briefs,
Technology Utilization Reports and Notes,
and Technology Surveys.

Details on the availability of these publications may be obtained from:

SCIENTIFIC AND TECHNICAL INFORMATION DIVISION

NATIONAL AERONAUTICS AND SPACE ADMINISTRATION
Washington, D.C. 20546